

A neoantigen vaccine generates antitumour immunity in renal cell carcinoma

<https://doi.org/10.1038/s41586-024-08507-5>

Received: 19 February 2024

Accepted: 10 December 2024

Published online: 5 February 2025

Open access

 Check for updates

David A. Braun^{1,2,3}✉, Giorgia Moranzoni⁴, Vipheaviny Chea⁵, Bradley A. McGregor^{3,6}, Eryn Blass³, Chloe R. Tu⁷, Allison P. Vanasse⁵, Cleo Forman³, Juliet Forman³, Alexander B. Afeyan^{3,6}, Nicholas R. Schindler², Yiwen Liu⁷, Shuqiang Li⁵, Jackson Southard⁵, Steven L. Chang^{6,8}, Michelle S. Hirsch^{6,9}, Nicole R. LeBoeuf^{6,10,11}, Oriol Olive³, Ambica Mehndiratta³, Haley Greenslade³, Keerthi Shetty³, Susan Klaeger¹², Siranush Sarkizova¹², Christina B. Pedersen^{4,13}, Matthew Mossanen^{6,8}, Isabel Carulli⁵, Anna Tarren⁵, Joseph Duke-Cohan⁵, Alexis A. Howard⁵, J. Bryan Iorgulescu^{3,9,12,19}, Bohoon Shim⁷, Jeremy M. Simon^{7,14}, Sabina Signoretti^{5,9,12,15}, Jon C. Aster^{6,9}, Liudmila Elagina¹², Steven A. Carr¹², Ignaty Leshchiner^{12,16}, Gad Getz^{12,17}, Stacey Gabriel¹², Nir Hacohen^{12,15,17}, Lars R. Olsen⁴, Giacomo Oliveira^{3,6,12}, Donna S. Neuberg⁷, Kenneth J. Livak⁵, Sachet A. Shukla^{5,20}, Edward F. Fritsch^{3,12}, Catherine J. Wu^{3,6,12,21}✉, Derin B. Keskin^{3,4,5,6,12,18,21}, Patrick A. Ott^{3,6,12,21} & Toni K. Choueiri^{3,6,21}✉

Personalized cancer vaccines (PCVs) can generate circulating immune responses against predicted neoantigens^{1–6}. However, whether such responses can target cancer driver mutations, lead to immune recognition of a patient's tumour and result in clinical activity are largely unknown. These questions are of particular interest for patients who have tumours with a low mutational burden. Here we conducted a phase I trial (ClinicalTrials.gov identifier NCT02950766) to test a neoantigen-targeting PCV in patients with high-risk, fully resected clear cell renal cell carcinoma (RCC; stage III or IV) with or without ipilimumab administered adjacent to the vaccine. At a median follow-up of 40.2 months after surgery, none of the 9 participants enrolled in the study had a recurrence of RCC. No dose-limiting toxicities were observed. All patients generated T cell immune responses against the PCV antigens, including to RCC driver mutations in *VHL*, *PBRM1*, *BAP1*, *KDM5C* and *PIK3CA*. Following vaccination, there was a durable expansion of peripheral T cell clones. Moreover, T cell reactivity against autologous tumours was detected in seven out of nine patients. Our results demonstrate that neoantigen-targeting PCVs in high-risk RCC are highly immunogenic, capable of targeting key driver mutations and can induce antitumour immunity. These observations, in conjunction with the absence of recurrence in all nine vaccinated patients, highlights the promise of PCVs as effective adjuvant therapy in RCC.

Neoantigens are derived from tumour-specific mutations and represent important targets of T cell-mediated antitumour immunity⁷. PCVs directed at neoantigens have the potential to steer antitumour immune responses towards cancer-cell-specific epitopes⁸, with the goal of improving on-target efficacy and reducing off-target immune toxicity. However, the optimal disease setting and the most effective neoantigen targets remain largely unknown. In melanoma, a cancer type with a high tumour mutational burden (and consequently a large number of potential neoantigen targets for a vaccine), PCVs have been shown to be feasible, safe and capable of inducing long-term antigen-specific T cell memory responses^{4–6}. In a phase II study of patients with high-risk, resected melanoma, the addition of a PCV to standard-of-care adjuvant PD-1 blockade (pembrolizumab) reduced tumour recurrence or death by 44%¹. However, for tumours with a low mutational burden, PCVs have faced implementation challenges in both initial manufacturing and in the effective generation of vaccine-specific immune responses^{2,3}. In a

phase I trial of a PCV as adjuvant therapy for pancreatic adenocarcinoma², 16 out of 32 enrolled patients were able to receive the planned PCV therapy, and 8 of those 16 patients generated immune responses to vaccination. However, immune responses to more than one targeted neoantigen was seen in only 4 out of 8 patients (50% of immune responders and 25% of all patients who received the vaccine)². Notably, at the 18-month median follow-up, no disease recurrence was detected among the 8 patients who had an immune response to the neoantigen vaccine, whereas disease recurrence was observed at the expected rate in patients who did not mount a vaccine response. These observations highlight both the challenges and the potential of PCVs as adjuvant therapy in tumours with a low mutational burden.

RCC is a prevalent disease, and these tumours have a relatively low mutational burden⁹ with defined cancer driver mutations¹⁰. Therefore, RCC is highly representative of tumours with a low mutational burden. Immune-based therapies can be effective in RCC, as reflected by the

A list of affiliations appears at the end of the paper.

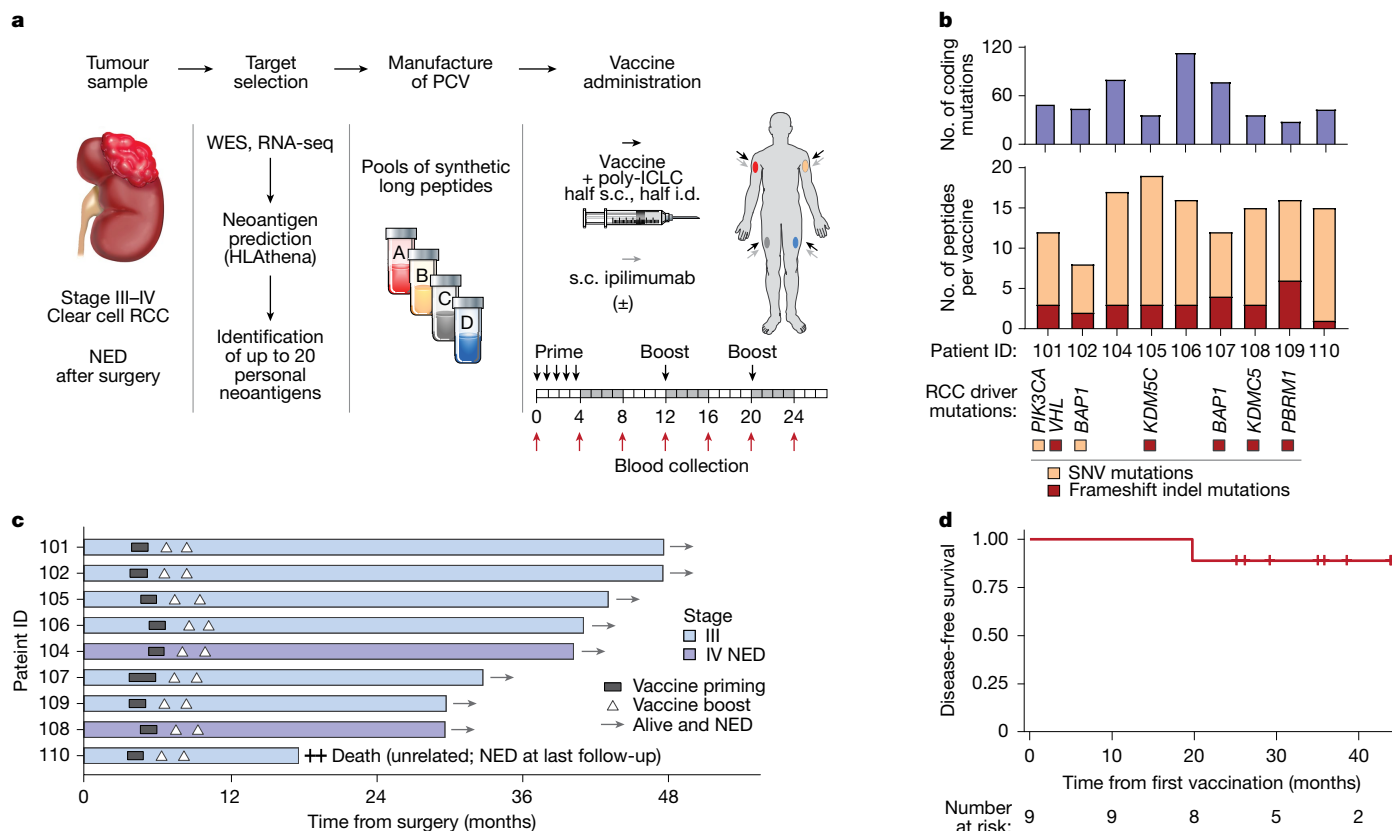


Fig. 1 | Vaccine manufacturing process and clinical outcomes. **a**, Overview of the design and administration of the neoantigen-targeting PCV for clear cell RCC. At each site, each individual received half of the vaccine subcutaneously (under the skin; s.c.) and the other half intradermally (between the layers of the skin; i.d.). The immunotherapy drug ipilimumab was also administered to a subset of individuals (indicated by ±). Blood was collected at several time points over 24 weeks (red arrows). NED, no evidence of disease; WES, whole exome sequencing. **b**, Summary of the vaccine manufacturing process,

including the number of high-quality coding mutations in each tumour (top), the number of neoantigen vaccine peptides administered for each patient (middle) and RCC-specific driver mutations targeted by the vaccine (bottom). ID, identifier; SNV, single nucleotide variant. **c**, Swimmer's plot showing the timelines and outcomes of each patient enrolled in the trial, starting at nephrectomy. **d**, Kaplan–Meier estimate of disease-free survival, starting at initial vaccine dose. The illustrations in **a** were created by Sarah Pyle and Steven Moskowitz.

proven antitumour activity of both historical (cytokine-based) and contemporary (immune-checkpoint-inhibitor-based) immunotherapies¹¹. Although neoantigens may represent a class of T cell target antigens in RCC¹², a greater number of neoantigens has not been associated with improved responsiveness to immune checkpoint inhibitors in this disease. This is in contrast to malignancies with high mutational burdens such as melanoma, lung cancer or microsatellite-instability-high colorectal cancer^{10,13}. In the adjuvant setting in RCC, a phase III study demonstrated that patients had an improved disease-free survival and overall survival with pembrolizumab¹⁴; however, many patients still experienced disease recurrence. Furthermore, three other adjuvant and perioperative phase III trials of immune checkpoint inhibitors, including atezolizumab, nivolumab, and nivolumab plus ipilimumab, did not demonstrate any clinical benefit in the adjuvant setting^{15–17}. Thus, there remains a high unmet clinical need to improve outcomes after surgery for patients with high-risk, resected RCC.

Overall, the low mutation burden, defined cancer driver mutations, existing signal for immunotherapy efficacy and ongoing unmet clinical need of RCC means that RCC represents an ideal disease setting to investigate the role of adjuvant PCV therapy. Furthermore, vaccination studies of RCC in which autologous whole tumour cells¹⁸, tumour-associated antigen peptides^{19,20} or a single neoantigen-containing peptide^{21,22} were assessed have provided a foundation for studying multi-epitope, neoantigen-targeting PCVs in this disease. To this end, we conducted an investigator-initiated phase I clinical trial of peptide-based, neoantigen-targeting PCVs in high-risk, fully resected RCC and a

comprehensive analysis of immune activity following this therapy (Fig. 1a; ClinicalTrials.gov identifier NCT02950766).

No disease recurrence after vaccination

For all nine patients who met eligibility criteria for analyses (Extended Data Fig. 1a), a PCV was successfully manufactured and administered. The baseline characteristics of the study participants were typical for high-risk RCC, with 7 out of 9 patients with high-grade disease (grade 3) and 2 out of 9 patients with metastatic (stage IV) disease at the time of enrolment (Table 1). The RCC tumours had a median of 45 high-quality coding mutations per sample (range of 29–114; Fig. 1b and Supplementary Table 1). A median of 15 neoantigen-containing peptides were successfully synthesized, allocated to 1 out of 4 peptide pools and administered as peptide pools to each patient (range of 8–19 individual peptides; Supplementary Table 2). All patients were vaccinated with at least one peptide that resulted from a frameshift insertion and deletion (indel; range of 1–6) that led to novel open reading frames. Seven out of the nine patients were successfully vaccinated with a peptide that contained a neoantigen derived from a cancer driver mutation, including common RCC gene mutations in *VHL*, *PBRM1*, *BAP1*, *KDM5C* and *PIK3CA* and other pan-cancer driver mutations (Supplementary Table 2). Five patients (identifier 101, 102, 104, 105 and 106) received the PCV with ipilimumab subcutaneously administered adjacent to the vaccination site (cohort 1), whereas the other patients received the vaccine alone (cohort 2).

Table 1 | Characteristics of patients at baseline

Characteristic	Value n (%)
Age (years)	
Mean ± s.d.	63.2 ± 8.1
Median	65.5
Range	50.4 – 75.7
Sex	
Female	2 (22)
Male	7 (78)
ECOG performance status score	
0	7 (78)
1	2 (22)
Tumour histology	
Clear cell	9 (100)
Sarcomatoid and/or rhabdoid differentiation	0 (0)
Stage	
III	7 (78)
IV	2 (22)
ISUP grade	
Grade 2	1 (11)
Grade 3	8 (89)
Primary tumour size	
4–7 cm	4 (44)
7–10 cm	3 (33)
>10 cm	2 (22)

A total of nine patients were enrolled and reported in these cohorts of the study. ECOG, Eastern Cooperative Group; ISUP, International Society of Urological Pathology.

The most common adverse events were low-grade injection-site reactions (in 100% of patients) and transient flu-like symptoms (in 8 out of 9 patients) (Table 2). No patient experienced a grade 3 or higher (dose-limiting) toxicity. With a median follow-up of 40.2 months from the time of surgery, none of the 9 vaccinated patients experienced a recurrence of RCC (Fig. 1c). One patient died from mental-health-related complications unrelated to RCC or to treatment. At a median follow-up of 34.7 months from initiation of the vaccination, the median disease-free survival was not reached (Fig. 1d). Direct comparisons with randomized phase III trials of adjuvant PD-1 axis blockade^{16,23} with similar patient eligibility criteria were not possible given the limited sample size of the current study. However, overall, patients treated with the PCVs had favourable clinical outcomes (Extended Data Fig. 1b).

PCVs are immunogenic in all patients

The PCVs were immunogenic in all nine patients (Fig. 2a, Extended Data Figs. 2 and 3a and Supplementary Table 2), with five out of nine patients generating vaccine-specific immune responses to all four peptide pools. Although the timing of the peak immune response varied from 8 to 24 weeks across participants, in 6 out of the 9 patients, the highest ex vivo T cell response was observed at 24 weeks after vaccination (4 weeks after completing the second booster dose). In detail, there was a median peak response of 477 spot-forming units per 10⁶ peripheral blood mononuclear cells (PBMCs) per peptide pool (range of 88–1,051). After in vitro stimulation and deconvolution of the immune responses against peptide pools, patients demonstrated immune reactivity against a median of 7 neoantigen vaccine peptides (range of 1–14). No substantial differences were observed in the kinetics or peak magnitude of the immune responses between the cohorts of patients who

Table 2 | Summary of treatment-related adverse events

Event	Grade 1 n (%)	Grade 2 n (%)
Fatigue	1 (11)	0
Flu-like symptoms	6 (67)	2 (22)
Injection site reaction	7 (78)	2 (22)
Malaise	1 (11)	0
Increased alanine aminotransferase	1 (11)	0
Decrease white blood cell count	2 (22)	0
Decreased neutrophil count	1 (11)	0
Dry skin	1 (11)	0

did or did not receive subcutaneous ipilimumab with the PCV. The majority of the T cell responses originated from CD4⁺ cells (98.7%), had an antigen-experienced, memory phenotype (PD-1⁺CD45RO⁺) and were polyfunctional (that is, produced 2 or more effector cytokines; 65.8% of T cell responses) (Fig. 2b and Extended Data Figs. 3b and 4a–d).

We further investigated whether vaccination against cancer driver mutations could lead to immune responses. In patient 101, a peptide that contained a frameshift mutation from the most common RCC driver gene *VHL* was highly immunogenic (Fig. 2c). Six patients were vaccinated with a total of seven peptides that encompassed one of the most common RCC driver mutations (*VHL*, *PBRM1*, *BAP1*, *KDM5C* and *PIK3CA*); six out of seven of these peptides induced an immune response following in vitro stimulation (Fig. 2d, Extended Data Figs. 2b and 3a and Supplementary Table 2). Across all pan-cancer driver mutations, 11 out of 17 were immunogenic (65%), and 50 out of 112 (44%) of passenger mutations were immunogenic (Fig. 2e, Extended Data Figs. 2b and 3a and Supplementary Table 2). For all peptides, no pre-existing immune responses were detected, and no clear association was observed between immunogenicity and clonality, gene expression or predicted human leukocyte antigen (HLA) class I allele binding affinity (Extended Data Fig. 4e–i).

Vaccination also induced broad and durable changes in circulating plasma proteins, including increases in cytokines supportive of T cell differentiation and effector function (for example, IL-12 and IL-18), markers of T cell activation (for example, CD27, CD28 and CD70) and markers of cytotoxicity (for example, granzyme A) (Fig. 2e, Extended Data Fig. 5 and Supplementary Table 3). Of note, markers of angiogenesis (for example, VEGFA), T cell suppression (for example, PD-1 and LAG3) and suppressive myeloid states (for example, CSF1) also increased over the course of vaccination. These findings support the presence of a broad and coordinated remodelling of immune responses following vaccination.

PCVs increase skin-infiltrating cytotoxic T lymphocytes

All nine patients developed inflammatory skin reactions at the injection sites. We performed biopsies at adjacent sites immediately before initiating vaccine priming (week 0) and from the injection sites 48–72 h after receiving the final vaccine priming dose (week 4) (Fig. 3a and Table 2). We performed single-cell transcriptomic analyses (single-cell RNA sequencing (scRNA-seq) and T cell receptor sequencing (TCR-seq); Supplementary Table 4) of skin-infiltrating immune cells from these biopsy samples. There were broad increases in the absolute number of infiltrating myeloid and lymphoid cell populations (Fig. 3b and Extended Data Fig. 6), and no substantial differences were noted between the cohorts of patients who did or did not receive ipilimumab (Extended Data Fig. 7).

Previous neoantigen peptide vaccines were subcutaneously delivered^{3,4}. The PCVs in this trial were administered intradermally and

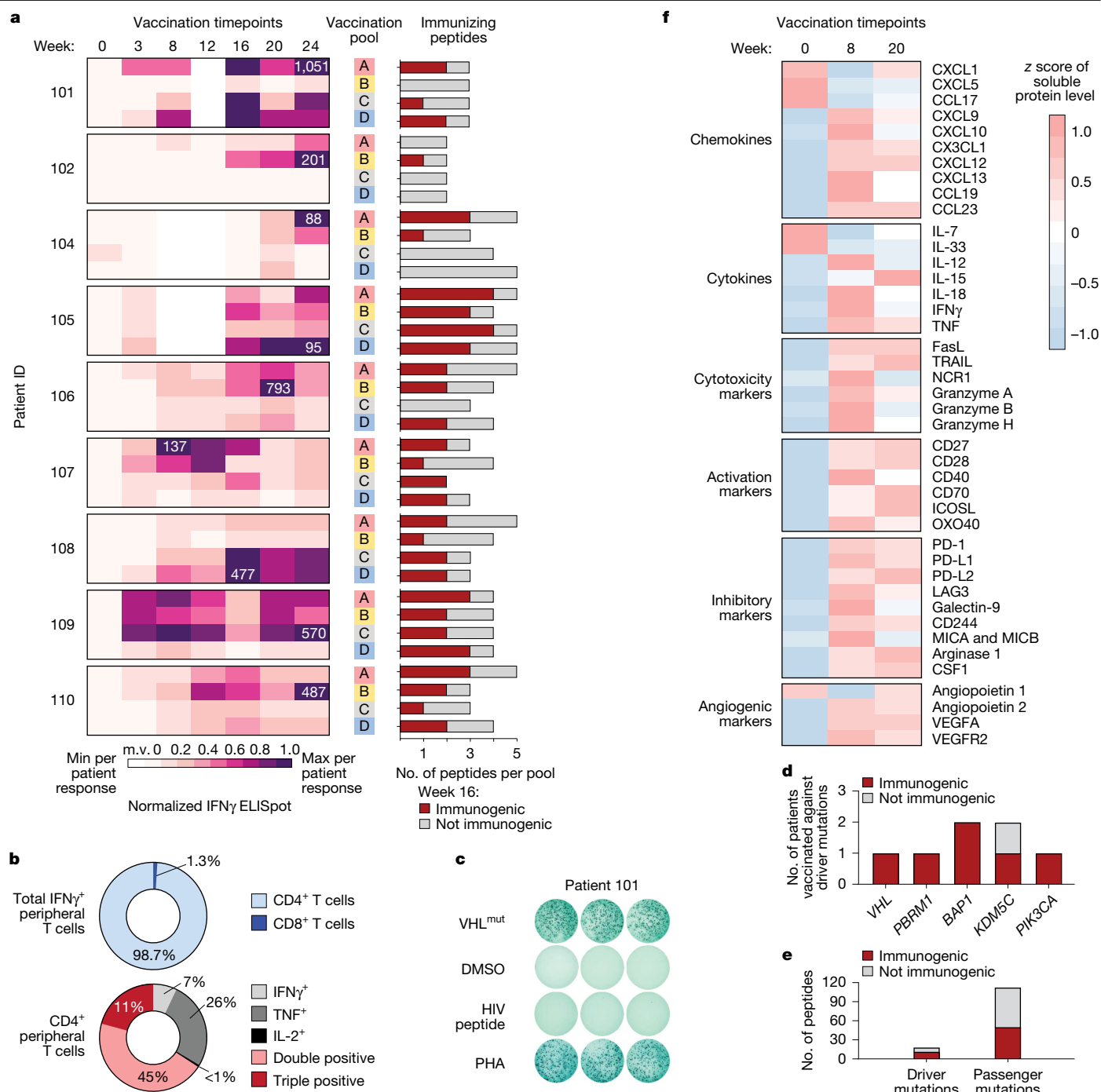


Fig. 2 | Vaccine immunogenicity and targetability of driver mutations.

a, Peripheral T cell immune responses following vaccination, measured using IFN γ ELISpot assays. Left, heatmap showing the dynamics of ex vivo T cell responses for each patient and each peptide pool. m.v. denotes missing values. White numbers in the heatmap indicate the absolute magnitude of the maximum per patient response, in spot-forming units per 10⁶ PBMCs. Right, the number of immunogenic individual peptides in each pool following in vitro stimulation. **b**, Summary of flow cytometry immunophenotyping and intracellular cytokine staining for all patients with assessable responses in the study cohort.

subcutaneously (half the dose administered for each delivery route), with the goal of engaging a broader repertoire of antigen-presenting cells in both the dermis and epidermis²⁴. In the myeloid compartment, there was a relative decrease in the proportion of these antigen-presenting cells (Langerhans cells and dendritic cell populations) in the skin after vaccination ($P = 0.016$; Fig. 3c), which could

c, Example IFN γ ELISpot images against an RCC driver mutation (VHL) from patient 101 PBMCs at week 16 following in vitro stimulation with a vaccine peptide pool, with dimethylsulfoxide (DMSO) and HIV peptides as negative controls, and phytohaemagglutinin (PHA) as a positive control, in triplicate. VHL^{mut}, mutant VHL peptide. **d**, Per patient immunogenicity of the five common RCC driver mutations in this study. **e**, Immunogenicity of pan-cancer driver and passenger mutations. **f**, Heatmap showing the median normalized levels of circulating plasma proteins before and after vaccination. Normalized protein expression for each soluble factor (z score).

potentially reflect the migration of antigen-presenting cells away from the injection site to the draining lymph node²⁵. However, further study is needed. Nevertheless, it may be that the changes observed are partially mediated by the inclusion of poly-ICLC in the vaccines. This adjuvant engages TLR3 and MDA5 and contributes to dendritic cell maturation and migration to the draining lymph node^{26,27}.

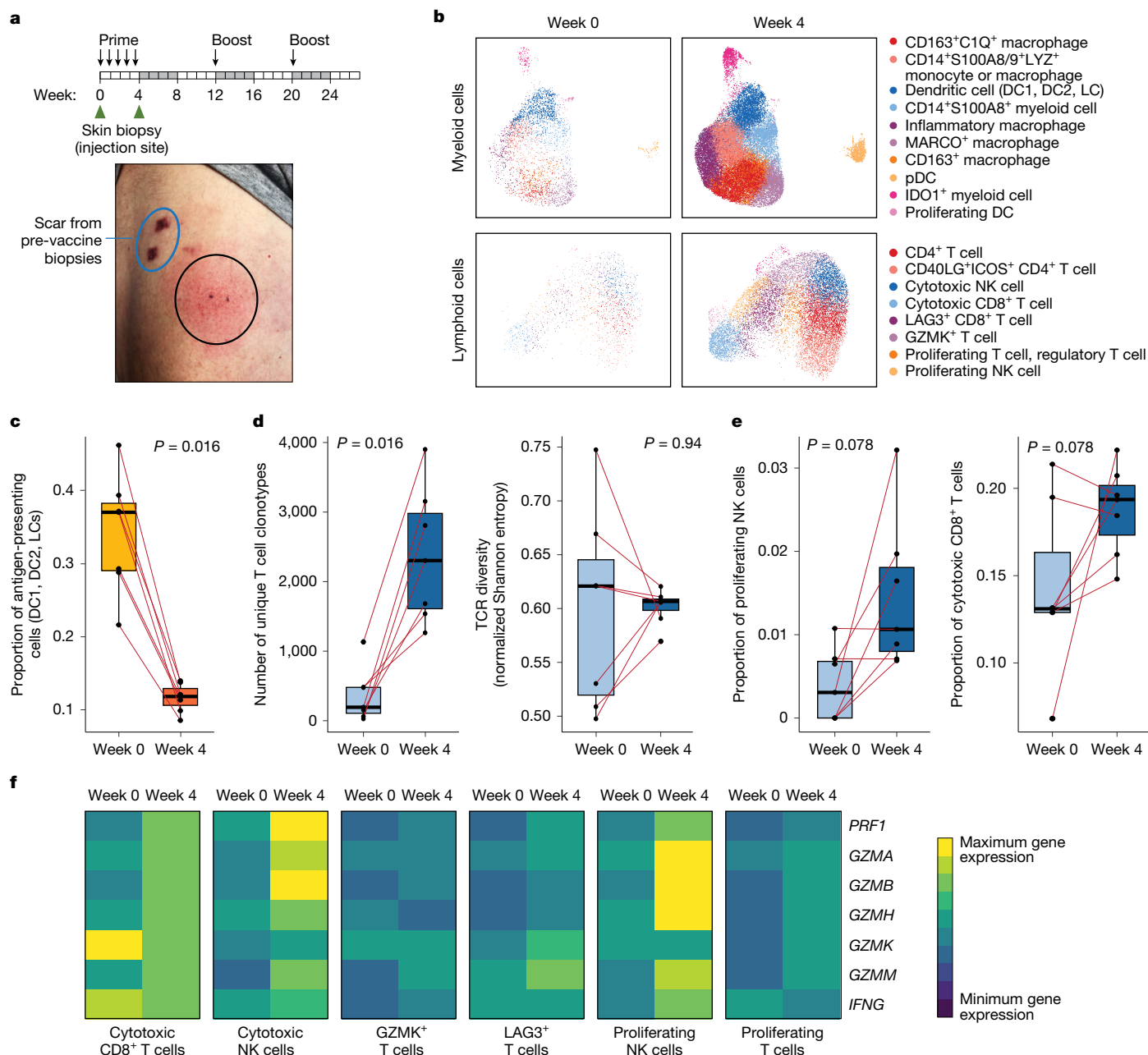


Fig. 3 | Vaccine-induced changes in skin-infiltrating immune cells. **a**, Top, schematic of skin assessments. Bottom, example of an injection-site reaction after vaccination, 48 h after priming. **b**, Uniform manifold approximation and projection (UMAP) representations of scRNA-seq data of skin-infiltrating myeloid and lymphoid cells before (week 0) and after vaccination (week 4) ($n = 9$ patients). **c**, Boxplot of the proportion of antigen-presenting cells (conventional dendritic cell (DC) subsets DC1 and DC2, and Langerhans cells (LCs)) before and after vaccination. **d**, Boxplots of the number of unique T cell clonotypes and TCR diversity before and after vaccination. **e**, Boxplots of

cytotoxic lymphoid populations before and after vaccination, proliferating NK cells and cytotoxic CD8⁺ T cells. **f**, Heatmap showing the relative change in expression of cytotoxicity genes in lymphoid subsets before and after vaccination. For **c–e**, P values were calculated using two-sided paired Wilcoxon test; $n = 7$ paired samples, as $n = 2$ patients had insufficient material at baseline for scRNA-seq; boxplot hinges represent 25th to 75th percentiles, central lines represent the medians, the whiskers extend to lowest and highest values no greater than 1.5 \times the interquartile range away from the 25th and 75th percentiles, and the dots indicate outliers.

Among skin-infiltrating T cells, although the overall TCR diversity was unchanged following vaccination ($P = 0.94$), the number of unique T cell clonotypes increased ($P = 0.016$; Fig. 3d), a result consistent with an absolute increase in overall T cell infiltration. Among lymphoid cells, the relative proportion of cytotoxic T cell and proliferating natural killer (NK) cell populations trended towards an increase with vaccination ($P = 0.078$ for both; Fig. 3e). Furthermore, in these cytotoxic cell populations, the expression of effector cytokine and cytotoxicity genes increased, including *PRF1*, *GZMB* and *IFNG* (Fig. 3f).

PCVs induce durable antitumour immunity

We investigated whether PCVs could lead to durable expansion of vaccine-specific T cells and recognition of the patient's own tumour. To infer vaccine-expanded T cell clones, we used TCR-seq to identify circulating T cell clones that were tenfold greater in peripheral blood specimens (through bulk TCR β sequencing) collected during or following vaccination compared with the pretreatment timepoint (Methods). Vaccine specificity was further confirmed in biopsy

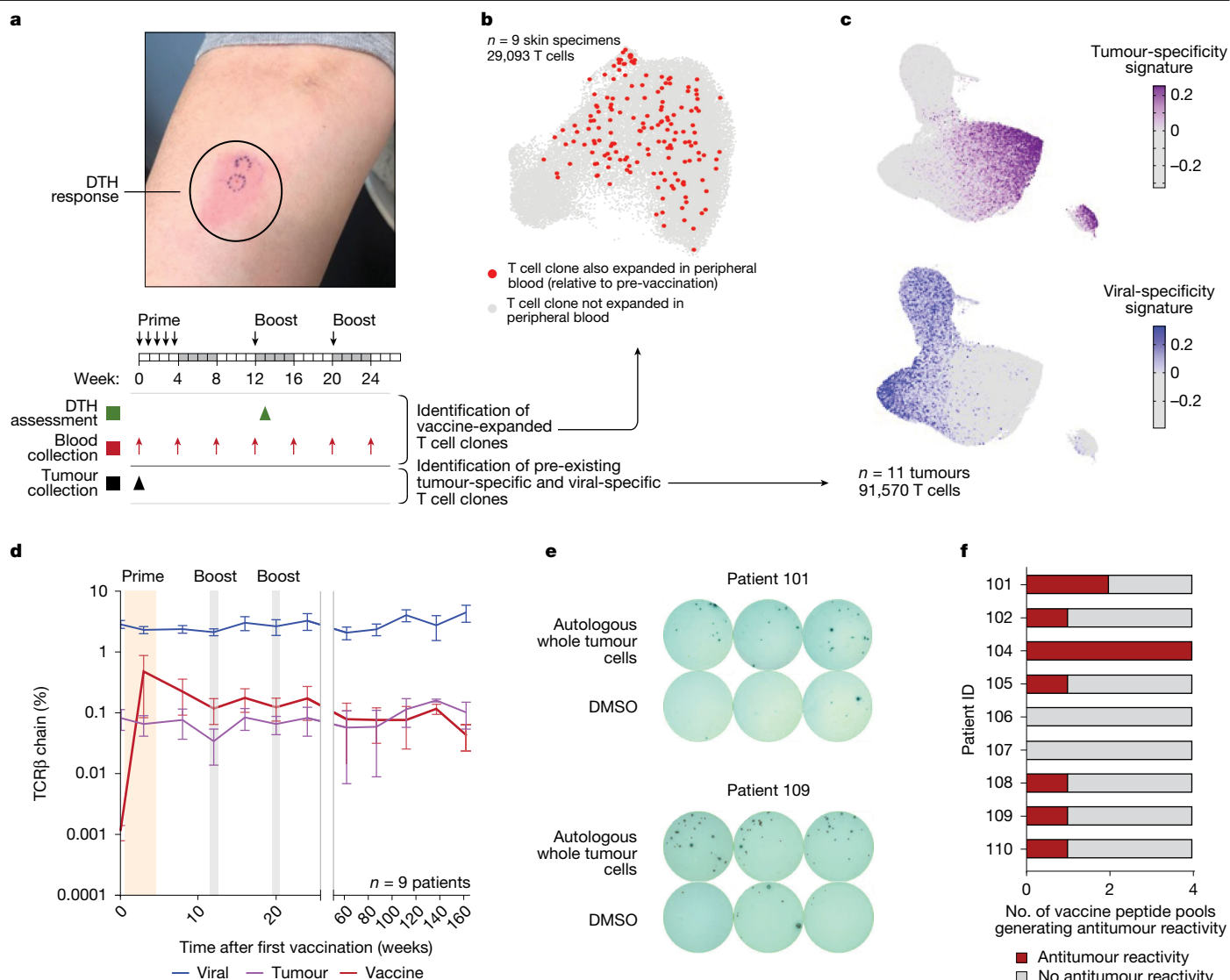


Fig. 4 | Vaccination induces T cell expansion and antitumour reactivity. **a**, Schematic depicting sample collection (bottom) and an example image of DTH assessment (top). **b**, UMAP representation of week-13 cutaneous DTH assessment. T cell clones that were highly expanded in the peripheral blood after vaccination were also found in the skin following DTH assessment. **c**, UMAP representation of tumour-infiltrating T cells, which demonstrates the gene expression score for tumour-specificity or viral specificity. The $n = 11$ tumours includes primary tumours from all 9 patients and metastatic tumours from the 2 patients with stage IV disease. **d**, Circulating TCR dynamics during and after vaccination, which demonstrates the relative stability of pre-existing

specimens collected following cutaneous delayed-type hypersensitivity (DTH) testing, which were profiled by scRNA-seq and TCR-seq (Fig. 4a,b and Supplementary Table 5). Across skin biopsy samples from the 9 patients and evaluation of 29,093 T cells with available TCR data, paired with longitudinal peripheral blood TCR-seq analyses from the 9 patients, we identified 98 vaccine-expanded T cell clones (Fig. 4b and Extended Data Fig. 8). In parallel, to identify pre-existing putative tumour-specific and viral-specific T cell clones, we measured the expression of previously validated specificity-associated gene signatures²⁸ in single-cell transcriptomes that we generated from T cells that infiltrated the baseline RCC tumours from the nine patients (Fig. 4c and Extended Data Fig. 9a–f). Pre-existing tumour-specific and viral-specific T cell clones remained relatively constant throughout treatment. By contrast, following vaccination, we observed a rapid

tumour-specific and viral-specific clones and the induction of vaccine-expanded T cell clones that persist following vaccination ($n = 9$ patients; error bars are s.e.m.). **e**, Example IFN γ ELISpot images of PBMCs at week 16, which demonstrate that post-vaccine peripheral T cells, expanded against neoantigen-peptides derived from RCC driver mutations (PIK3CA^{mut} for patient 101; PBRM1^{mut} for patient 109), are capable of recognizing autologous tumours (assays were performed in triplicate; DMSO was used as a negative control). **f**, The number of neoantigen peptide pools, per patient, that generated antitumour immune reactivity.

(within 3 weeks), substantial (mean of 166-fold) and durable (up to 3 years) expansion of new T cell clonotypes (Fig. 4d and Extended Data Fig. 8). The clonotype expansion predominantly occurred in CD4 T cells (Extended Data Fig. 8a,c), a result in line with the primarily CD4 T cell response observed by flow cytometry (Fig. 2b). Furthermore, the number of vaccine-expanded CD4 clonotypes (but not CD8 clonotypes) correlated with the IFN γ response, as assessed using ELISpot assays ($R = 0.8$, $P = 0.017$; Extended Data Fig. 9g and Supplementary Table 6).

Following vaccination, peripheral T cells expanded against vaccine peptides that contained RCC driver mutations in *VHL*, *PBRM1* and *BAP1* could directly recognize autologous tumour cells (Fig. 4e and Extended Data Fig. 10). Overall, antitumour reactivity was detected in 77.8% of patients (median of 1 peptide pool per patient; range of 0–4 peptide pools per patient; Fig. 4f and Supplementary Table 2).

Discussion

Neoantigen-targeting PCVs have held great promise, but inherent challenges with cancer vaccines remain, including antigen selection, effective T cell priming and overcoming an immunosuppressive tumour microenvironment²⁹. In this prospective trial of high-risk, resected RCC, none of the patients experienced a recurrence of RCC after a median follow-up of 40.2 months from surgical resection and 34.7 months from initiation of the PCV. Our study revealed several notable observations. First, despite RCC being a tumour with a low mutational burden, we successfully manufactured a multi-epitope vaccine for every patient enrolled in the trial. Second, most of the patients received a vaccine against neoantigens derived from mutations in major RCC driver genes, and these were highly immunogenic³⁰. Third, the vaccine antigens were immunogenic in all patients, typically against multiple epitopes, which led to polyfunctional memory T cell responses. Vaccination rapidly and durably expanded T cell clonotypes, with expansion persisting years after the last vaccine dose. Moreover, in most patients, the PCV resulted in immune reactivity against autologous tumour cells.

The current study builds on a foundation of previous vaccination studies of patients with RCC. A previous phase III study showed that adjuvant whole tumour cell vaccination improved progression-free survival^{31–33}. However, concerns about study design were raised and the programme was ultimately discontinued^{31–33}. Before the development of technologies that enabled PCVs to target neoantigens, a study of peptide vaccination against overexpressed or tumour-associated antigens did not show substantial benefit in the adjuvant setting¹⁹. These observations highlight the challenges of tumour-associated antigen vaccines, including the difficulty in overcoming central tolerance mechanisms that are necessary to generate effective antitumour immunity⁸. In an early study of neoantigen vaccination in RCC, a single-epitope vaccine targeting mutant VHL showed meaningful immune responses in four out of five evaluable patients²². Although this study provided early proof-of-principle for targeting neoantigens, there were limitations in the antigen-prediction tools available at the time and in the ability to target only a single antigen. Moreover, it was conducted in the setting of active metastatic disease in a number of study participants.

Our study highlights the important role of disease setting for implementing PCVs. In macrometastatic settings with a large disease burden, neoantigen vaccines have had modest efficacy across a range of solid tumours^{34,35}. In the adjuvant setting, however, in which only micrometastatic disease would be present, PCVs could have an essential role in clearing residual tumour burden^{2,4,36}. Our study therefore underscores the post-surgical adjuvant setting as an ideal context for PCVs, as the minimal disease setting presents the possibility of effective consolidative and curative therapy. More broadly, this work supports the concept of vaccines as an important addition to therapeutic combinations that first minimize disease burden, including the post-surgical and post-chemotherapy settings, which can both reduce tumour burden and mitigate cancer-mediated immunosuppression³⁷.

Given the highly immunosuppressive nature of the tumour microenvironment in advanced RCC³⁸, additional immunotherapy combinations will probably be required to maximize antitumour immune responses. Our initial hypothesis was that local delivery of ipilimumab might improve T cell priming in the local draining lymph nodes while avoiding systemic toxicities. Although the addition of subcutaneously administered ipilimumab was well tolerated, it did not seem to substantially change the magnitude or phenotype of the peripheral immune response in the immediate post-vaccination time period. This result must be interpreted with some caution, as future studies may still identify a role for CTLA4 blockade as a co-therapy for neoantigen-targeting PCVs. In our study, ipilimumab did affect the relative abundance of skin-infiltrating immune cells, particularly the antigen-presenting cells at the injection site. Furthermore, although CTLA4 blockade may

have more limited short-term effects, it is possible that it may affect long-term T cell quality, including an effective memory T cell population. Finally, we note that the total administered dose of ipilimumab in our study (2.5 mg per injection site) was substantially lower than the conventional systemic dose used in RCC or melanoma. Therefore, when locally delivered, higher doses of ipilimumab may produce more favourable results³⁹.

Moving forward, other immunological co-therapies could be considered. PD-1 pathway blockade, which forms the foundation of systemic therapy for metastatic RCC^{40–44} and is the only approved type of adjuvant immunotherapy in RCC¹⁴, is a natural partner to combine with neoantigen vaccination in the adjuvant setting (as has been effectively done in melanoma³⁶). However, the timing of PD-1 blockade relative to vaccination should be optimized to effectively prime T cells to boost effector function while preserving longer term immunological memory^{45,46}. Alternatively, our studies of serial plasma samples suggest other avenues for combination therapies designed to overcome circulating programmes induced by the PCV that may be counterproductive for antitumour immunity. Following vaccination, we observed an increase in angiogenesis factors, suppressive myeloid factors and multiple inhibitory T cell checkpoints. The PCV activates T cells, and T cell activation itself can result in the upregulation of inhibitory checkpoints such as PD-1 (ref. 47). Furthermore, the inclusion of poly-ICLC in the vaccine may broadly activate innate immunity, which can lead to the production of pro-angiogenic factors (such as VEGFA) by activated myeloid cells^{48,49} and interferon that could stimulate the expression of inhibitory ligands, including soluble PD-L1 (refs. 50,51). Thus, these changes may reflect counter-regulatory mechanisms that are increased following innate immune and T cell activation⁵², and knowledge of these induced pathways could provide a pathway for future rational combination trials that target these suppressive pathways and augment vaccine efficacy.

As observed in previous neoantigen vaccine studies^{3,4,6}, our PCVs induced a predominantly CD4⁺ T cell response. CD4⁺ T cells are increasingly being recognized as having an important role in generating effective antitumour immunity. CD4⁺ T cells can have a supporting role by providing CD40L on dendritic cells, which then activates them to enable effective priming of CD8⁺ T cells⁵³ or necessary activation of already primed T cells in the tumour⁵⁴. Through both direct effects on CD8⁺ T cells and indirect effects mediated by antigen-presenting cells, CD4⁺ T cells can augment CD8⁺ T cell migration, phenotype, differentiation and effector activity through the production of effector cytokines and expression. CD4⁺ T cells may also have a more direct antitumour effect through the production of effector cytokines, such as IFN γ , and potentially through direct cytotoxic activity^{53,55}. Therefore, the primarily CD4⁺ T cell responses observed in many neoantigen-targeting PCV studies probably make important contributions to antitumour immunity.

Although the initial immunological activity and clinical results of our small phase I study are encouraging, additional larger-scale studies will be required to confirm these findings and to fully understand the potential clinical efficacy of this approach. Larger-scale randomized trials of neoantigen-targeting PCVs are anticipated to provide important information about clinical activity. However, thus far, they frequently lack substantial immunological analyses required for proper interpretation. In this context, we assert that the generation of a 'comprehensive analysis set', as achieved in our study, is necessary to build a foundation on which to interpret future large-scale PCV studies of RCC. Furthermore, this initial study only included patients with the clear cell subtype, but approximately 25% of patients with kidney cancer have variant histology tumours (that is, non-clear cell RCC), and improving outcomes for these patients remains an unmet clinical need⁵⁶.

It is noteworthy that the PCVs (with or without locally delivered ipilimumab) were substantially less toxic than adjuvant immune checkpoint inhibition. In our study, no patients experienced a grade 3 or higher

adverse event. Although this finding must be interpreted with caution given the small sample size of our study, it does stand in contrast to the adjuvant pembrolizumab experience in RCC, in which 18.6% of patients encountered a grade 3 or higher toxicity and 21.1% had discontinued treatment because of side effects⁵⁷. The favourable toxicity profile of PCVs highlights the potential beneficial role for these neoantigen-targeting vaccines in RCC, either as monotherapy or in combination with immune checkpoint inhibition. Furthermore, the immunological efficacy and encouraging clinical outcomes in this tumour type with a low mutational burden support the broader investigation of PCVs as adjuvant therapies for solid tumours.

Overall, these results provide support the feasibility of creating a highly immunogenic personalized neoantigen vaccines in tumours with a low mutational burden. Such an approach, which includes vaccination against key disease driver mutations, can lead to effective antitumour immunity in solid tumours.

Online content

Any methods, additional references, Nature Portfolio reporting summaries, source data, extended data, supplementary information, acknowledgements, peer review information; details of author contributions and competing interests; and statements of data and code availability are available at <https://doi.org/10.1038/s41586-024-08507-5>.

- Weber, J. S. et al. Individualised neoantigen therapy mRNA-4157 (V940) plus pembrolizumab versus pembrolizumab monotherapy in resected melanoma (KEYNOTE-942): a randomised, phase 2b study. *Lancet* **403**, 632–644 (2024).
- Rojas, L. A. et al. Personalized RNA neoantigen vaccines stimulate T cells in pancreatic cancer. *Nature* **618**, 144–150 (2023).
- Keskin, D. B. et al. Neoantigen vaccine generates intratumoral T cell responses in phase Ib glioblastoma trial. *Nature* **565**, 234–239 (2019).
- Ott, P. A. et al. An immunogenic personal neoantigen vaccine for patients with melanoma. *Nature* **547**, 217–221 (2017).
- Hu, Z. et al. Personal neoantigen vaccines induce persistent memory T cell responses and epitope spreading in patients with melanoma. *Nat. Med.* **27**, 515–525 (2021).
- Sahin, U. et al. Personalized RNA mutanome vaccines mobilize poly-specific therapeutic immunity against cancer. *Nature* **547**, 222–226 (2017).
- Schumacher, T. N. & Schreiber, R. D. Neoantigens in cancer immunotherapy. *Science* **348**, 69–74 (2015).
- Hacohen, N., Fritsch, E. F., Carter, T. A., Lander, E. S. & Wu, C. J. Getting personal with neoantigen-based therapeutic cancer vaccines. *Cancer Immunol. Res.* **1**, 11–15 (2013).
- Lawrence, M. S. et al. Mutational heterogeneity in cancer and the search for new cancer-associated genes. *Nature* **499**, 214–218 (2013).
- Braun, D. A. et al. Interplay of somatic alterations and immune infiltration modulates response to PD-1 blockade in advanced clear cell renal cell carcinoma. *Nat. Med.* **26**, 909–918 (2020).
- Kashima, S. & Braun, D. A. The changing landscape of immunotherapy for advanced renal cancer. *Urol. Clin. North Am.* **50**, 335–349 (2023).
- Rooney, M. S., Shukla, S. A., Wu, C. J., Getz, G. & Hacohen, N. Molecular and genetic properties of tumors associated with local immune cytolytic activity. *Cell* **160**, 48–61 (2015).
- Bruni, D., Angell, H. K. & Galon, J. The immune contexture and Immunoscore in cancer prognosis and therapeutic efficacy. *Nat. Rev. Cancer* **20**, 662–680 (2020).
- Choueiri, T. K. et al. Adjuvant pembrolizumab after nephrectomy in renal-cell carcinoma. *N. Engl. J. Med.* **385**, 683–694 (2021).
- Motzer, R. J. et al. Adjuvant nivolumab plus ipilimumab versus placebo for localised renal cell carcinoma after nephrectomy (CheckMate 914): a double-blind, randomised, phase 3 trial. *Lancet* **401**, 821–832 (2023).
- Pal, S. K. et al. Adjuvant atezolizumab versus placebo for patients with renal cell carcinoma at increased risk of recurrence following resection (IMmotion010): a multicentre, randomised, double-blind, phase 3 trial. *Lancet* **400**, 1103–1116 (2022).
- Allaf, M. et al. LBA67 phase III randomized study comparing perioperative nivolumab (nivo) versus observation in patients (Pts) with renal cell carcinoma (RCC) undergoing nephrectomy (PROSPER, ECOG-ACRIN EA8143), a National Clinical Trials Network trial. *Ann. Oncol.* **33**, S1432–S1433 (2022).
- Jocham, D. et al. Adjuvant autologous renal tumour cell vaccine and risk of tumour progression in patients with renal-cell carcinoma after radical nephrectomy: phase III, randomised controlled trial. *Lancet* **363**, 594–599 (2004).
- Rini, B. I. et al. IMA901, a multi-peptide cancer vaccine, plus sunitinib versus sunitinib alone, as first-line therapy for advanced or metastatic renal cell carcinoma (IMPRINT): a multicentre, open-label, randomised, controlled, phase 3 trial. *Lancet Oncol.* **17**, 1599–1611 (2016).
- Hongo, F. et al. Phase I/II study of multi-peptide cancer vaccine IMA901 after single-dose cyclophosphamide in Japanese patients with advanced renal cell cancer with long-term follow up. *Int. J. Urol.* **30**, 176–180 (2023).
- Achtar, M. S. et al. Vaccine therapy with tumor specific mutated VHL peptides in adult cancer patients with renal cell carcinoma. *J. Clin. Oncol.* **22**, 2589 (2004).
- Rahma, O. E. et al. A pilot clinical trial testing mutant von Hippel-Lindau peptide as a novel immune therapy in metastatic renal cell carcinoma. *J. Transl. Med.* **8**, 8 (2010).
- Powles, T. et al. Pembrolizumab versus placebo as post-nephrectomy adjuvant therapy for clear cell renal cell carcinoma (KEYNOTE-564): 30-month follow-up analysis of a multicentre, randomised, double-blind, placebo-controlled, phase 3 trial. *Lancet Oncol.* **23**, 1133–1144 (2022).
- Liard, C. et al. Intradermal immunization triggers epidermal Langerhans cell mobilization required for CD8 T-cell immune responses. *J. Invest. Dermatol.* **132**, 615–625 (2012).
- Shklovskaya, E., Roediger, B. & Fazekas de St Groth, B. Epidermal and dermal dendritic cells display differential activation and migratory behavior while sharing the ability to stimulate CD4⁺ T cell proliferation in vivo. *J. Immunol.* **181**, 418–430 (2008).
- Steinman, R. M. Decisions about dendritic cells: past, present, and future. *Annu. Rev. Immunol.* **30**, 1–22 (2012).
- Longhi, M. P. et al. Dendritic cells require a systemic type I interferon response to mature and induce CD4⁺ Th1 immunity with poly IC as adjuvant. *J. Exp. Med.* **206**, 1589–1602 (2009).
- Oliveira, G. et al. Phenotype, specificity and avidity of antitumour CD8⁺ T cells in melanoma. *Nature* **596**, 119–125 (2021).
- Sellars, M. C., Wu, C. J. & Fritsch, E. F. Cancer vaccines: building a bridge over troubled waters. *Cell* **185**, 2770–2788 (2022).
- Cancer Genome Atlas Research Network. Comprehensive molecular characterization of clear cell renal cell carcinoma. *Nature* **499**, 43–49 (2013).
- Bedke, J. et al. Targeted therapy in renal cell carcinoma: moving from molecular agents to specific immunotherapy. *World J. Urol.* **32**, 31–38 (2014).
- Kubler, H. & Vieweg, J. Vaccines in renal cell carcinoma. *Semin. Oncol.* **33**, 614–624 (2006).
- Kommu, S. Renal-cell carcinoma: vaccination and risk of tumour progression. *Lancet* **363**, 1557 (2004).
- Ott, P. A. et al. A phase Ib trial of personalized neoantigen therapy plus anti-PD-1 in patients with advanced melanoma, non-small cell lung cancer, or bladder cancer. *Cell* **183**, 347–362 (2020).
- Braiteh, F. et al. Abstract CT169: a phase Ia study to evaluate RO7198457, an individualized Neoantigen Specific immunoTherapy (iNeST), in patients with locally advanced or metastatic solid tumors. *Cancer Res.* **80**, CT169 (2020).
- Khattak, A. et al. Abstract CT001: a personalized cancer vaccine, mRNA-4157, combined with pembrolizumab versus pembrolizumab in patients with resected high-risk melanoma: efficacy and safety results from the randomized, open-label phase 2 mRNA-4157-P201/Keynote-942 trial. *Cancer Res.* **83**, CT001 (2023).
- Liu, M. et al. Improved T-cell immunity following neoadjuvant chemotherapy in ovarian cancer. *Clin. Cancer Res.* **28**, 3356–3366 (2022).
- Braun, D. A. et al. Progressive immune dysfunction with advancing disease stage in renal cell carcinoma. *Cancer Cell* **39**, 632–648 (2021).
- Palmer, C. D. et al. Individualized, heterologous chimpanzee adenovirus and self-amplifying mRNA neoantigen vaccine for advanced metastatic solid tumors: phase 1 trial interim results. *Nat. Med.* **28**, 1619–1629 (2022).
- Motzer, R. et al. Lenvatinib plus pembrolizumab or everolimus for advanced renal cell carcinoma. *N. Engl. J. Med.* **384**, 1289–1300 (2021).
- Choueiri, T. K. et al. Nivolumab plus cabozantinib versus sunitinib for advanced renal-cell carcinoma. *N. Engl. J. Med.* **384**, 829–841 (2021).
- Motzer, R. J. et al. Avelumab plus axitinib versus sunitinib for advanced renal-cell carcinoma. *N. Engl. J. Med.* **380**, 1103–1115 (2019).
- Rini, B. I. et al. Pembrolizumab plus axitinib versus sunitinib for advanced renal-cell carcinoma. *N. Engl. J. Med.* **380**, 1116–1127 (2019).
- Motzer, R. J. et al. Nivolumab plus ipilimumab versus sunitinib in advanced renal-cell carcinoma. *N. Engl. J. Med.* **378**, 1277–1290 (2018).
- Pauken, K. E. et al. The PD-1 pathway regulates development and function of memory CD8⁺ T cells following respiratory viral infection. *Cell Rep.* **31**, 107827 (2020).
- Verma, V. et al. PD-1 blockade in subprimed CD8 cells induces dysfunctional PD-1^{CD38} cells and anti-PD-1 resistance. *Nat. Immunol.* **20**, 1231–1243 (2019).
- Agata, Y. et al. Expression of the PD-1 antigen on the surface of stimulated mouse T and B lymphocytes. *Int. Immunol.* **8**, 765–772 (1996).
- Azari, Z. et al. The role of immune cells in therapeutic angiogenesis: concepts in tissue engineering. *Curr. Opin. Biomed. Eng.* **28**, 100470 (2023).
- Frantz, S., Vincent, K. A., Feron, O. & Kelly, R. A. Innate immunity and angiogenesis. *Circ. Res.* **96**, 15–26 (2005).
- Patoukakis, N., Wang, Q., Strauss, L. & Boussiotis, V. A. Revisiting the PD-1 pathway. *Sci. Adv.* **6**, eabd2712 (2020).
- Frigola, X. et al. Soluble B7-H1: differences in production between dendritic cells and T cells. *Immunol. Lett.* **142**, 78–82 (2012).
- Sharpe, A. H. & Pauken, K. E. The diverse functions of the PD1 inhibitory pathway. *Nat. Rev. Immunol.* **18**, 153–167 (2018).
- Borst, J., Ahrends, T., Babala, N., Melief, C. J. M. & Kastenmuller, W. CD4⁺ T cell help in cancer immunology and immunotherapy. *Nat. Rev. Immunol.* **18**, 635–647 (2018).
- Espinosa-Carrasco, G. et al. Intratumoral immune triads are required for immunotherapy-mediated elimination of solid tumors. *Cancer Cell* **42**, 1202–1216 (2024).
- Saxena, M., van der Burg, S. H., Melief, C. J. M. & Bhardwaj, N. Therapeutic cancer vaccines. *Nat. Rev. Cancer* **21**, 360–378 (2021).
- Albiges, L., Flippot, R., Rioux-Leclercq, N. & Choueiri, T. K. Non-clear cell renal cell carcinomas: from shadow to light. *J. Clin. Oncol.* <https://doi.org/10.1200/JCO.2018.79.2531> (2018).
- Choueiri, T. K. et al. Overall survival with adjuvant pembrolizumab in renal-cell carcinoma. *N. Engl. J. Med.* **390**, 1359–1371 (2024).

Publisher's note Springer Nature remains neutral with regard to jurisdictional claims in published maps and institutional affiliations.



Open Access This article is licensed under a Creative Commons Attribution-NonCommercial-NoDerivatives 4.0 International License, which permits any non-commercial use, sharing, distribution and reproduction in any medium or format, as long as you give appropriate credit to the original author(s) and the source, provide a link to the Creative Commons licence, and indicate if you modified the licensed material. You do not have permission under this licence to share adapted material derived from this article or parts of it. The images or other third party material in this article are included in the article's Creative Commons licence, unless indicated otherwise in a credit line to the material. If material is not included in the article's Creative Commons licence and your intended use is not permitted by statutory regulation or exceeds the permitted use, you will need to obtain permission directly from the copyright holder. To view a copy of this licence, visit <http://creativecommons.org/licenses/by-nc-nd/4.0/>.

© The Author(s) 2025

¹Section of Medical Oncology, Department of Internal Medicine, Yale School of Medicine, New Haven, CT, USA. ²Center of Molecular and Cellular Oncology, Yale Cancer Center, Yale School of Medicine, New Haven, CT, USA. ³Department of Medical Oncology, Dana-Farber Cancer Institute, Boston, MA, USA. ⁴Section for Bioinformatics, Department of Health Technology, Technical University of Denmark, Kongens Lyngby, Denmark. ⁵Translational Immunogenomics

Laboratory, Dana-Farber Cancer Institute, Boston, MA, USA. ⁶Harvard Medical School, Boston, MA, USA. ⁷Department of Data Science, Dana-Farber Cancer Institute, Boston, MA, USA. ⁸Department of Urology, Brigham and Women's Hospital, Boston, MA, USA. ⁹Department of Pathology, Brigham and Women's Hospital, Boston, MA, USA. ¹⁰Center for Cutaneous Oncology, Dana-Farber Brigham and Women's Cancer Center, Boston, MA, USA. ¹¹Department of Dermatology, Brigham and Women's Hospital, Boston, MA, USA. ¹²Broad Institute of MIT and Harvard, Cambridge, MA, USA. ¹³Center for Genomic Medicine, Rigshospitalet–Copenhagen University Hospital, Copenhagen, Denmark. ¹⁴Department of Biostatistics, Harvard T. H. Chan School of Public Health, Boston, MA, USA. ¹⁵Department of Oncologic Pathology, Dana-Farber Cancer Institute, Boston, MA, USA. ¹⁶Section of Computational Biomedicine, Department of Medicine, Boston University School of Medicine, Boston, USA. ¹⁷Massachusetts General Hospital Cancer Center, Boston, MA, USA. ¹⁸Department of Computer Science, Metropolitan College, Boston University, Boston, MA, USA. ¹⁹Present address: Molecular Diagnostics Laboratory, Department of Hematopathology, Division of Pathology and Laboratory Medicine, The University of Texas MD Anderson Cancer Center, Houston, TX, USA. ²⁰Present address: Department of Hematopoietic Biology and Malignancy, The University of Texas MD Anderson Cancer Center, Houston, TX, USA. ²¹These authors contributed equally: Catherine J. Wu, Derin B. Keskin, Patrick A. Ott, Toni K. Choueiri. [✉]e-mail: david.braun@yale.edu; catherine_wu@dfci.harvard.edu; toni_choueiri@dfci.harvard.edu

Methods

Study design

Patients with presumed high-risk RCC who provided informed consent were screened for eligibility and enrolled in a single-centre, phase I clinical trial approved by the Dana-Farber Harvard Cancer Center Institutional Review Board (NCT02950766). The study was conducted in accordance with the Declaration of Helsinki. Eligibility criteria for final registration included histologically confirmed RCC, American Joint Committee on Cancer (AJCC) stage (eighth edition) stage III (pT3 and/or N1) or fully resected stage IV (pT4 and/or M1 with no evidence of disease). The following additional criteria were applied: Eastern Cooperative Group (ECOG) performance status of 0 or 1; normal organ and bone marrow function; no previous treatment with immunomodulatory agents or RCC-directed cancer vaccine; no previous non-immune systemic therapy within the previous 6 months; no concomitant therapy for cancer or autoimmunity; no history of autoimmune disease or immunodeficiency; and no other non-oncology vaccine within 4 weeks before the first dose of vaccine until 8 weeks after the last dose (with an exception made for vaccination against the SARS-CoV-2 virus). Patients were enrolled in the first cohort (vaccine plus 2.5 mg of subcutaneous ipilimumab at each vaccine site) and the second cohort (vaccine alone) between March 2019 and September 2021. A third cohort of patients treated with vaccine plus 5 mg of subcutaneous ipilimumab at each vaccine site continued enrolment until December 2022 with follow-up ongoing and is not included in this analysis.

The primary objectives of the study were the safety and tolerability of administering the PCV together with locally delivered (subcutaneous) ipilimumab, and the maximum tolerated dose of locally delivered ipilimumab. Secondary objectives were the induction of neoantigen-specific cellular immune responses following vaccination and the proportion of patients alive without recurrence at 2 years after surgery. Each PCV consisted of 4 pools, each containing up to 5 synthetic long peptides targeting neoantigens (300 µg per peptide), admixed with 0.5 mg poly-ICLC (Hiltonol, Oncovir) per pool. Each peptide pool was assigned a non-rotating limb for administration (for example, pool A was always administered in the right thigh). For each administration, each peptide pool was separated into two syringes, and half of the vaccine dose was administered subcutaneously and half intradermally (using separate syringes). For patients who received ipilimumab (patients 101, 102, 104, 105 and 106), it was subcutaneously administered within 1 cm of the vaccine site. The vaccine was administered on days 1, 4, 8, 15 and 22 for vaccine priming and then on weeks 12 and 20 for the booster phase.

Clinical assessments

The safety of treatment was assessed during each vaccine administration and additionally 1 week after the priming phase (day 29), on weeks 8, 13, 16, 21 and 24 and then every 12 weeks during the follow-up phase (up to 2 years). Adverse events were categorized and graded using the NCI Common Terminology Criteria for Adverse Events (CTCAE v.4.0). Dose-limiting toxicity was defined as the following specific toxicities that occurred within 7 weeks of treatment initiation: (1) grade 3–4 toxicity except transient (≤ 72 h) flu-like symptoms, grade 3 nausea that returns to grade 2 or lower within 48 h or grade 3 rash that resolves to grade 2 or lower within 14 days; (2) grade 3–4 laboratory abnormality that persists for more than 7 days or requires hospitalization or medical intervention; (3) any grade 3–4 toxicity that is considered by the investigator to be dose-limiting; (4) any death related to study treatment. To monitor for disease recurrence, imaging (CT chest, abdomen and pelvis, CT chest and MRI abdomen and pelvis, or PET–CT) was performed at baseline, every 8 weeks up to 24 weeks, then every 12 weeks during the follow-up period (up to 2 years) and then at a frequency decided on by the treating physician (typically every 6 months). Recurrence was assessed using RECIST (v.1.1) guidelines.

Clinical outcomes and safety

Clinical outcomes and safety data are reported until the clinical data cut-off of 7 July 2023. Disease-free survival is reported as the time (in months) of disease recurrence or death from the start of treatment. Analyses and visualizations were generated using the R packages survival (v.3.5.5) and survminer (v.0.4.9). For qualitative comparisons with other recent, randomized clinical trials of immune checkpoint inhibitor as adjuvant therapy for RCC, KEYNOTE-564 (ref. 23) and IMmotion-010 (ref. 16) were selected as the therapeutic settings, and the eligibility criteria of those studies closely matched the current PCV study, specifically adjuvant therapy for high-risk RCC after surgical resection and inclusion of patients with fully resected metastatic disease (termed ‘M1 NED’). The Kaplan–Meier curves for KEYNOTE-564 and IMmotion-010 were reconstructed as previously described⁵⁸ using Digitizelt software (v.2.5.9) together with the IPDfromKM package in R (v.0.1.10).

Patient samples

At the time of surgical resection, grossly viable sections of RCC tumour were identified by board-certified, expert trained genitourinary pathologists, and tumour tissue was placed into formalin and into cold DMEM medium (Gibco) on ice. To manufacture the PCV, formalin-fixed tumour tissue was processed and embedded in paraffin blocks at the Dana-Farber Harvard Cancer Center Specialized Histopathology Core, a facility certified by the College of American Pathologists (CAP) and the Clinical Laboratory Improvement Amendments (CLIA). Slides stained with haematoxylin and eosin were prepared from each formalin-fixed paraffin-embedded (FFPE) block to confirm the presence of clear cell RCC. For the two patients with stage IV (metastatic disease), both patients had a single metastatic site in the abdomen, and this was surgically resected at the time of nephrectomy. Separately, FFPE blocks from the primary tumour in the kidney and from the metastatic site were prepared and both were used for the design of the vaccine. The block with the highest tumour purity and lowest necrosis was selected for preparation of FFPE thick sections (scrolls), which was transported to the Broad Institute for isolation of DNA and RNA for sequencing studies. All material used for production of the clinical vaccine followed a strict chain of custody, with multiple standard checkpoints in place to ensure the correct identity of the specimen.

For research (non-clinical) analyses, fresh tumour tissue and adjacent non-malignant kidney tissue were placed in separate tubes containing DMEM on ice. Sections of tumour and normal tissue were enzymatically and mechanically dissociated as previously described³⁸. Fresh tissue was minced with scalpels to 1–2 mm³ fragments and incubated in digestion medium containing 0.11 U ml⁻¹ collagenase D (Roche), 0.56 U ml⁻¹ dispase (Stemcell), 50 U ml⁻¹ DNase I (NEB), 5 mM CaCl₂ and HBSS (Life Technologies) at 37 °C for 10 min with agitation. Single-cell suspensions of tumour or normal kidney were then cryopreserved in 10% DMSO plus 90% FBS for downstream use.

Peripheral blood samples were obtained before or at the time of surgery for HLA typing and for germline DNA sequencing. Once eligibility was confirmed, clinical HLA class I and II typing was performed by the BWH Tissue Typing Laboratory. For immune monitoring of PBMCs, leukaphereses were performed before vaccination (within 10 days) and at week 16 following vaccine initiation. Peripheral blood samples (K₂-EDTA tubes) were also collected at weeks 3, 8, 12, 20 and 24 following vaccine initiation (with additional specific samples collected at the discretion of the investigator). PBMCs were isolated by Ficoll (GE Healthcare) density centrifugation and then cryopreserved for downstream analyses. The plasma layer following density centrifugation was frozen at –80 °C for downstream analyses of circulating soluble protein.

For analyses of skin-infiltrating immune cells, two 5-mm punch biopsy samples were obtained from non-sun-exposed skin (right proximal thigh for the pretreatment and post-vaccine priming samples, and right volar forearm for the cutaneous DTH assessment). Skin samples

Article

were minced using scalpels, incubated in digestion enzymes (Miltenyi Whole Skin Dissociation kit, using enzyme P and enzymes A + D), incubated at 37 °C for 2 h with agitation and further dissociated using a Miltenyi gentleMACS (program h_skin_01). The single-cell suspension was then enriched for CD45⁺ immune cells through immunomagnetic purification (Miltenyi anti-CD45 microbeads) and immediately used for downstream analyses.

Generation of neoantigen-targeting PCVs

The creation of each PCV involved WES of tumour tissue and peripheral blood, RNA-seq of tumour, somatic mutation calling, identification of target neoantigens and then synthesis, pooling and preparation of the vaccine product. For the two patients with metastatic disease, tumour material from both the primary tumour and the single resected metastatic site underwent sequencing and analysis for vaccine design.

For WES of tumour and normal blood, FFPE tumour scrolls and a peripheral blood sample were transported to the Broad Institute Clinical Research Sequencing Platform (CRSP), a CLIA licensed (22D2055652) and CAP accredited (8707596) laboratory for the standard somatic WES test. DNA derived from FFPE samples was extracted using a Qiagen DNA FFPE QIAamp kit per the recommended protocol. Deparaffinization solution (DPS) from the kit was added to the samples and incubated on a heat block at 56 °C per the manufacturer's recommendations. Following the DPS treatment, buffer ATL and proteinase K from the kit were added to the samples and incubated on a heat block overnight at 56 °C and then at 90 °C in a heat block for 1 h the following day. The lysate was then transferred to a new tube, and RNase A, buffer AL and ethanol were added. The lysate was transferred to a QIAamp spin column, and wash buffers included in the kit were added. The sample was finally eluted with the provided ATE buffer and stored at 4 °C for downstream processing. Following extraction of total DNA from blood and tumour tissue using these standardized procedures, library construction was performed. Library construction was performed as previously described⁵⁹, with the following modifications (as previously reported⁶⁰): the initial genomic DNA input into shearing was reduced from 3 µg to 20–250 ng in 50 µl of solution. For adapter ligation, Illumina paired-end adapters were replaced with palindromic forked adapters (Integrated DNA Technologies) with unique dual-indexed molecular barcode sequences to facilitate downstream pooling. For end repair and A-tailing, adapter ligation and library enrichment PCR, Kapa HyperPrep reagents were used in a 96-reaction kit format. For the post-enrichment SPRI clean-up, the library concentration was maximized by reducing the elution volume to 30 µl to maximize library concentration. Libraries were pooled (up to 96 samples), and hybridization and capture were performed using an Illumina's Nextera Exome kit. The following modifications were made from the manufacturer's protocol: (1) all libraries in a library construction plate were pooled before hybridization; (2) a skirted PCR plate was used to facilitate automation (Agilent Bravo liquid handling system) instead of the Midi plate from Illumina's Nextera Exome kit. After post-capture enrichment, library pool quantification was performed using qPCR (automated assay on the Agilent Bravo) probes specific to the ends of the adapters (KAPA Biosystems). Libraries were normalized to 2 nM and then cluster amplification was performed according to the manufacturer's protocol (Illumina) using exclusion amplification chemistry and flowcells. The flowcells were analysed using RTA (v.2.7.3 or later). Each pool of whole exome libraries was sequenced on paired 76 cycle runs on Illumina HiSeq or NovaSeq instruments with two 8-cycle index reads across the number of lanes (or equivalent) needed to meet coverage for all libraries in the pool. The anticipated read depth for most samples was >150× mean target coverage.

RNA-seq was performed to confirm the expression of putative neoantigens. For all patients, a separated portion of tumour tissue (FFPE scroll) was sent to the non-CLIA/CAP Broad Institute Genomics Platform. RNA derived from FFPE samples was extracted using a Qiagen AllPrep DNA/RNA FFPE kit per the recommended protocol. DPS from

the kit was added to the samples and incubated at 56 °C per the manufacturer's recommendations. Following the DPS treatment, the samples were placed on a heat block at 37 °C to evaporate any residual buffer. Once all residual buffer was removed, buffer PKD and proteinase K from the provided kit were added and the samples incubated at 56 °C. The samples were then centrifuged to collect the DNA-containing pellet and RNA-containing supernatant. The RNA supernatant was transferred to a new tube and incubated on a heat block at 80 °C. Buffer RLT from the kit and ethanol was added to the lysate and was applied to a RNeasy MinElute spin column. A series of wash buffers and ethanol were applied to the bound RNA for purification. The sample was finally eluted with the provided RNase-free water and denatured at 65 °C and flash chilled on wet ice. The purified RNA was then stored at –80 °C for downstream processing. Following RNA extraction using these standardized procedures, transcriptome capture RNA-seq was performed using an optimized protocol for RNA from FFPE tissues (Broad Institute). Total RNA was quantified using a Quant-iT RiboGreen RNA Assay kit and normalized to 5 ng µl⁻¹. Following plating, 2 µl of ERCC controls (using a 1:1,000 dilution) were spiked into each sample. RNA quality was measured using a Caliper LabChip GX system, which was used to calculate a RIN-equivalent RNA quality score. The per cent of RNA fragments greater than 200 nucleotides were also quantified into a DV200 score. Using a TruSeq RNA Access Library Prep kit (Illumina), a stranded cDNA library was prepared from isolated RNA, which was then hybridized to a set of DNA oligonucleotide probes to enrich the library for mRNA transcript fragments. Flowcell cluster amplification and sequencing were performed according to the manufacturer's protocols using Illumina HiSeq or NovaSeq S2 instruments. Each run was a 76 bp paired-end with an eight-base index barcode read. Data were analysed using the Broad Picard Pipeline, which includes demultiplexing and data aggregation. Alignment was completed using the STAR alignment algorithm against human reference hg19. Transcriptome capture covers the RefSeq and GENCODE (v.12) databases to >98%.

When available, additional RNA-seq of purified tumour cells (that is, without other cells from the microenvironment) was performed. CA9-positive tumour cells were immunomagnetically purified (using Miltenyi anti-CA9 PE antibody and anti-PE microbeads) from freshly dissociated tumour and cultured for 48–72 h in OptiMEM GlutaMax medium (Gibco) containing 5% FBS, 1 mM sodium pyruvate, 100 U ml⁻¹ penicillin and streptomycin, 50 µg ml⁻¹ gentamicin, 5 µg ml⁻¹ insulin and 5 ng ml⁻¹ EGF. RNA was extracted using a Qiagen RNeasy kit, and RNA-seq of this low-input RNA was performed using a modified version of the Smart-seq2 protocol (using the NEBNext Single Cell/Low Input cDNA Synthesis and Amplification module) as previously described³.

Somatic mutations in WES data were detected using an implementation of the Cancer Genome Analysis WES Characterization pipeline (as previously implemented¹⁰; hereafter, referred to as the CGA pipeline) in a cloud-based analysis platform, Terra (<https://terra.bio/>). We used v.0.2 of the CGA pipeline. As quality-control steps, the CGA pipeline ran deTiN⁶¹ and ContEst⁶² for estimating tumour-in-normal and cross-patient contaminations, respectively. The pipeline applies multiple artefact filters such as the read-realignment filter by BLAT⁶³ and the read orientation bias filters followed by SNV and indel calling with MuTect⁶⁴ and Strelka⁶⁵. All somatic alterations were annotated using Oncotator⁶⁶. Tumour ploidy and purity were determined using ABSOLUTE⁶⁷, and this was used to assign clonality (cancer cell fraction) for each somatic mutation. RNA-seq data were quantified as previously described¹⁰. In brief, RNA-seq data were aligned to the human reference genome (hg19) and transcriptome (GENCODE v.19) using STAR (v.2.6.1)⁶⁸, and expression was quantified (transcripts per million) using RSEM (v.1.3.1)⁶⁹. All coding mutations were visualized using the Integrated Genomics Viewer (IGV v.2)⁷⁰. Each somatic mutation was categorized as high quality or green (variant read support in WES and RNA-seq), yellow (high quality in WES but not identified in RNA-seq) or red (likely artefact). Green-categorized mutations were prioritized

for downstream analyses, although yellow-categorized mutations were also included.

To predict neoantigens, the detected coding mutations were converted into peptide sequences, and the translated neoantigens (that is, peptides with missense mutations and indels) were sliced into 8, 9, 10 or 11 amino-acid lengths for HLA class I binding prediction. Antigen prediction was performed using HLAthena (v.0)⁷¹ and NetMHCpan (v.4)⁷² (eluted ligand rank). Each potential antigen was ranked as follows: (1) predicted strong binder (rank < 0.5) by both prediction models; (2) predicted strong binder by HLAthena only; (3) predicted strong binder by NetMHCpan only; (4) predicted weak binder (rank < 2) by both prediction models; (5) predicted weak binder by HLAthena only; (6) predicted weak binder by NetMHCpan only; (7) not a predicted binder.

For each patient, an epitope selection board (ESB) was convened, which consisted of investigators with expertise in RCC, genomics, immunobiology, cancer immunotherapies and peptide chemistry. The ESB selected up to 20 short epitopes based on mutation quality, antigen rank, cancer driver status (favouring driver over passenger mutations), expression (in bulk tumour or in the purified tumour RNA; favouring high expression), clonality (favouring clonal over subclonal mutations) and whether the somatic alteration was a frameshift indel capable of producing a novel open reading frame. The list of driver genes for this cohort was created on the basis of known cancer genes and significantly mutated genes in the Cancer Genome Atlas—clear cell kidney cancer cohort (TCGA-KIRC)³⁰ and PanCancer lists from the TumorPortal⁷³ (<http://www.tumorportal.org/>). Genes with detected somatic mutations were intersected with the driver gene list, and the nonsynonymous mutations in the driver genes were marked as driver mutations. For the two patients with metastatic disease, we prioritized neoantigens that were present in both the primary and the metastatic tumour. A small number of neoantigens were also selected that were present in only the primary tumour or in only the metastatic tumour. For the selected short epitopes, the ESB designed synthetic long peptides (15–33 amino acids in length) containing the peptide sequence flanking the short epitope, with a length and sequence intended to maximize synthesizability and solubility.

Good manufacturing practice peptides were synthesized using standard solid-phase synthetic peptide chemistry and purified by reverse-phase high-performance liquid chromatography (RP-HPLC; Neon Therapeutics for patients 101 and 102, Almac Sciences for the other patients). Each individual peptide was analysed using various qualified assays to assess appearance (visual), purity (RP-HPLC), identity (by mass spectrometry) and quantity. Peptides were combined into one of four pools containing up to five peptides (designed to maximize the diversity of predicted HLA class I binding allele and excluding peptides that did not demonstrate clear solutions; the assigned pool for each peptide is listed in Supplementary Table 2). Each peptide pool was sterile-filtered and underwent additional testing for sterility and the presence of endotoxin. On the day of administration. Each pool was thawed, mixed with poly-ICLC (Hiltonol, Oncovir) and separated into syringes for subcutaneous and intradermal administration, as described above.

For cutaneous DTH testing, 0.25 ml of each vaccine pool (containing 100 µg of each peptide and without poly-ICLC or ipilimumab) was combined (1 ml total volume), and 100 µl of this mixture of all vaccine peptides was intradermally administered in the right forearm 7–14 days after the week 12 vaccine priming dose. At 48–72 h following injection, the DTH site was assessed for erythema and induration, and biopsies were performed (two 5-mm punch biopsies) at the injection site and samples were processed in the same manner as other skin biospecimens, as described above.

Assessment of vaccine immunogenicity by IFN γ ELISpot

PBMCs containing circulating T cells were assessed for immune reactivity to vaccine peptide pools immediately after thawing and rest

(ex vivo), to individual vaccine peptides following in vitro stimulation with pools of peptides, and to autologous tumour cells following in vitro stimulation with individual peptides or peptide pools. All T cell culture and ELISpot methods (including plate development and analysis) were performed as previously described^{74,75}.

For assessing the dynamic ex vivo immunogenicity of vaccine peptide pools over the course of vaccination, PBMCs containing T cells spanning week 0 (before first vaccination) until week 24 (after vaccine initiation) were screened against pooled neoantigen vaccine peptides by ex vivo IFN γ ELISpot assays. Opaque ELISpot plates with 0.45 mm hydrophobic high protein binding immobilon-p membranes (Millipore) were wet with 35% ethyl alcohol. Wells were washed with distilled water three times. Plates were coated with anti-IFN γ antibody at 4 °C (1-DK1 Mabtech) and were then washed with PBS before stimulation. Cryopreserved PBMCs from the nine patients were thawed in complete DMEM medium supplemented with 10% human serum and rested overnight. The PBMCs were then plated at 2×10^5 cells per well and stimulated with 10 µg peptide pool. DMSO and/or 10 µg HIV peptides were used as negative controls. CMV, EBV and influenza-derived (CEF) peptide pools (Mabtech) and PHA (Gibco) were used as positive controls. Each stimulation was set up in triplicate and incubated for 18–24 h at 37 °C. Plates were developed using manufacturer's protocols. For each time-point, responses were background-subtracted (that is, the median of the negative controls were subtracted). Responses were defined as positive if they showed >55 spot-forming units per 10^6 PBMCs and at least threefold increase over baseline.

Neoantigen vaccine peptide pools were deconvoluted to identify immunogenic peptides by in vitro IFN γ ELISpot assays. To generate vaccine-pool-specific T cells, week 0 and week 16 PBMCs were plated in 24-well plates at 5×10^6 to 1×10^7 cells per well and stimulated with 10 µg ml⁻¹ vaccine peptide pools in DMEM medium supplemented with 10% human serum and 20 ng ml⁻¹ of IL-7 (PeproTech). On day 3, the T cells were cultured with DMEM medium supplemented with 10% human serum and 20 U ml⁻¹ of IL-2 (PeproTech). In vitro IFN γ ELISpot assays were performed 10–14 days after stimulation, after resting the T cells in cytokine-free medium overnight. For these assays, 3×10^4 cells were plated against 10 µg individual vaccine peptide (negative controls, DMSO and 10 µg of HIV; positive controls, CEF peptides and PHA). No reactivity was detected in week 0 PBMCs. For week 16 PBMCs, positive peptide responses were identified as those that were significantly increased compared with the negative control (DMSO; using a two-sided *t*-test and a significance threshold of 0.05, without adjustment for multiple comparisons) and that had at least threefold median increase in the number of IFN γ spot-forming units over the negative control.

T cells that were reactive to individual peptides and/or peptide pools were further assessed for reactivity to autologous tumour cells. Dissociated tumours (either all dissociated cells or tumour cells immunomagnetically enriched using anti-CA9 antibodies and Miltenyi microbeads) were either used directly or pre-stimulated with 250–2,000 units of IFN γ (PeproTech) 2–3 days before ELISpot assays were performed (to increase antigen presentation). For quantifying the tumour reactivity of T cells stimulated with vaccine peptide pools, 3×10^4 T cells were plated against 1×10^4 autologous (that is, patient-specific) unstimulated and IFN γ -stimulated (IFN γ ⁺) tumour cells. For individual immunogenic vaccine peptides, antigen-specific T cell lines derived from week 0 (control) and week 16 PBMCs were generated and cultured as described above. Antigen-specific T cell lines were then tested 10–14 days after stimulation using in vitro IFN γ ELISpot assays. To confirm immunogenicity and tumour reactivity, 3×10^4 T cells were plated with DMSO (negative control), against 10 µg of individual immunizing long peptides or against 1×10^4 tumour cells. Positive peptide (or peptide pool) responses were identified as those that were significantly increased compared with the negative control (DMSO; using a two-sided *t*-test and a significance threshold of 0.05,

Article

without adjustment for multiple comparisons) and that had at least threefold median increase in the number of IFN γ spot-forming units over the negative control.

Assessment of T cell immunophenotype and cytokine production by flow cytometry

PBMCs were thawed and rested overnight at 37 °C in RPMI (Life Technologies) containing 10% human serum (Sigma-Aldrich), 1% penicillin and streptomycin (Life Technologies) and 20 ng ml⁻¹ of IL-7 (PeproTech). The following day, PBMCs were stimulated with vaccine peptide pools (2 μ g ml⁻¹ per individual peptide) in complete R10 medium (RPMI, 10% FBS and 1% penicillin and streptomycin). After 1 h of co-culture at 37 °C, transport inhibitors GolgiStop and GolgiPlug were added. Following 5 h of incubation at 37 °C, samples were washed with 1 \times PBS and stained with live/dead dye in 1 \times PBS for 20 min at 4 °C. Samples were subsequently washed with staining buffer (1 \times PBS, 10% FBS and 1% penicillin and streptomycin). Fc receptors were blocked for 15 min at 4 °C with Human TruStain FcX in staining buffer. The following surface-staining antibodies were then added: CD4 (clone L200), CD8 (clone RPA-T8), CD45RO (clone UCHL1) and PD-1 (clone EH12.2H7). Following 30 min of incubation at 4 °C, samples were washed twice before fixation and permeabilization with CytoFix/CytoPerm for 15 min at 4 °C. Samples were then washed twice and resuspended in 1 \times Perm/Wash buffer to conduct intracellular staining with IFN γ (clone B27), TNF (clone Mab11), IL-2 (clone MQ1-17H12) and CD3 (clone UCHT1). Following 30 min of incubation at 4 °C, samples were washed twice with Perm/Wash, once with staining buffer and then resuspended in CytoFix fixation buffer until acquisition. All flow cytometry reagents were purchased from BD Biosciences or BioLegend. Data were acquired on a BD LSR Fortessa with FACSDiva and analysed using FlowJo (v.10.8.1). Background responses, as determined by DMSO control, were subtracted from peptide pools to determine the frequency of neoantigen-specific cytokine responses. Samples had to have at least 50 IFN γ ⁺ T cells to be included in the analysis. Furthermore, the frequency of IFN γ ⁺ cells had to be at least 1.5-fold higher than in the negative control, HIV gag, to be included. When CD4⁺ and CD8⁺ T cells did not meet these stringency thresholds, the results are reported as 'n.d.' for 'not detectable', and not include in the summary statistics. When these criteria were not met for CD8⁺ T cells specifically (but were for CD4⁺ T cells), the proportion of CD8⁺ T cells was set to zero for that sample. Finally, the HIV gag negative control was not available for assessments of samples from patient 110, and so although the individual results are reported in Extended Data Fig. 5, they are not included in the summary Fig. 2b.

Measurement of circulating soluble proteins

The levels of circulating cytokines, chemokines and other soluble plasma proteins before and during vaccination were quantified using an Olink Target 96 Immuno-Oncology assay. Stored plasma from week 0 (before vaccination), week 3 (during vaccine priming) and week 20 (before the second booster dose and 8 weeks after the previous vaccine administration) was transported to the Human Immune Monitoring Center at the Icahn School of Medicine at Mount Sinai for Olink analysis. All values are reported as normalized protein expression (in arbitrary units). For Supplementary Table 3, for each cytokine, the median value across all patients is reported. Statistical testing was performed using a two-sided paired Wilcoxon test, comparing pretreatment (week 0) with either week 3 or week 20 timepoints (excluding patient 104, who did not have pretreatment measurements available).

scRNA-seq and scTCR-seq

scRNA-seq and single-cell TCR-seq (scTCR-seq) were performed as previously described³⁸. All skin samples were processed immediately (that is, fresh) following dissociation, whereas tumour and normal kidney samples were thawed (after previously being cryopreserved). Dead cells were immunomagnetically depleted using a Dead Cell Removal

kit (Miltenyi), washed and resuspended in PBS with 0.04% BSA at a concentration of 1,000 cells per μ l. Approximately 17,000 cells were loaded onto a 10x Genomics Chromium instrument (10x Genomics). Libraries were prepared using a Chromium single cell 5' kit v.2 (for gene expression) and a Chromium single-cell human TCR amplification kit (for scTCR-seq). Following library construction, quality control and quantification, libraries were pooled and sequenced on an Illumina NovaSeq S4. The 10x Cell Ranger pipeline (v.6.1.2) was used for data demultiplexing, data alignment and count quantification and TCR clonotype assembly.

Analysis of scRNA-seq and scTCR-seq data from vaccine-site skin

scRNA-seq data were imported and read using a custom function built on the Seurat (v.4.3.0) pipeline⁷⁶. The function discriminates between raw and filtered Cell Ranger outputs, reads the 10x data, creates the Seurat object and calculates the mitochondrial content. For raw input Cell Ranger data, a filtering step that removes cells with nFeature_RNA < 5 was also performed, before returning the preprocessed Seurat object. Quality control was performed following the standard Seurat pipeline. Cells with fewer than 200 genes, fewer than 500 unique molecular identifiers (UMIs) and more than 20% mitochondrial content were excluded. Doublets were identified and removed using three different methods: doubletFinder⁷⁷ (v.2.0.3), scDblFinder⁷⁸ (v.1.12.0) and nFeature_RNA > 2,500. Any cells identified as doublets by any of these three methods were excluded from further analyses.

Following preprocessing, the skin data were harmonized using the package Harmony (v.0.1.1)⁷⁹ with a maximum iteration setting of 20. Thereafter, the skin data were clustered using Seurat's FindClusters function with default options, and the optimal clustering resolution was determined using the clustree function from the package clustree (v.0.5.0)⁸⁰. The immune subset was then identified and subsetted on the basis of expression of the immune marker *PTPRC* (which encodes CD45). The immune subset was further clustered using the methodology outlined above. Despite conservative doublet filtering, one cluster (cluster 9) was identified as consisting of doublet cells and removed from further analyses. Cluster 11, identified as keratinocytes and not immune cells, was also excluded.

Differential gene expression analysis was performed using the FindAllMarkers function from Seurat with standard options. The purpose of this analysis was to identify differentially expressed genes characterizing each immune cluster. After clustering the immune subset and performing differential gene expression analysis, myeloid and T cell populations were identified on the basis of canonical markers, including *CD33* and *CD3E* expression, respectively. After isolating myeloid and T cell compartments, each population was further clustered to identify T cell and myeloid subpopulations. Differential gene expression analysis was performed for each myeloid and T cell subcluster as described above.

To identify changes in populations during vaccination (that is, from week 0 before vaccination to week 4 following vaccine priming) and any impact of subcutaneous administration of ipilimumab (that is, comparing week 4 skin in patients who received vaccine alone versus those who received vaccine plus ipilimumab), we performed a population abundance analysis. Specifically, we focused on each subcluster in the myeloid and T cell compartments. The proportions for population abundance were calculated by dividing the number of cells in each subpopulation by the total number of the parent population (either T cells or myeloid cells) per sample. Significance of change in frequency over time (week 0 versus week 4) was assessed using a two-tailed, paired Wilcoxon test, whereas differences across treatment was determined by a two-tailed, unpaired Wilcoxon test. Two patients (105 and 107) were excluded from the paired analysis owing to the lack of samples at week 0 (too few immune cells for library construction and sequencing). Box-plots of population abundances are shown with the median, the 25th and 75th percentiles (box) and 1.5 \times the interquartile range (whiskers).

To determine any phenotypic changes that may occur in a specific population following vaccination, we performed differential gene expression analysis for each cluster (week 0 versus week 4) using the function FindMarkers from Seurat. Heatmaps were generated using the R package pheatmap (v.1.0.12).

For TCR diversity and clonotype analysis, we used the R package VDJdive (v.1.3.5)⁸¹. This package was used to assess the clonal repertoire diversity and abundance in the TCR sequences. Clonotype labels were assigned using the clonoStats function, with the following parameters: method = "EM", type = "TCR", assignment = TRUE, group = "sample". TCR diversity was calculated using the calculateDiversity function, using the normentropy method. This measure provides a normalized entropy score that quantifies the diversity of TCR clonotypes in each sample, based on a matrix of clonotype abundances, with higher scores indicating greater clonal diversity. The significance of the differences in the number of unique clonotypes and in TCR diversity between week 0 and week 4 skin-infiltrating T cells was assessed using a two-tailed paired Wilcoxon test.

Analysis of scRNA-seq and scTCR-seq data from tumour and normal kidney

scRNA-seq data preprocessing, harmonization and clustering and identification of T cell populations were performed as described above for the skin analysis. One cluster (cluster 15) was identified as a mitochondrial contaminant and removed from further analyses. Patient-specific TCR clonotypes were identified using TCR α and TCR β chains and CDR3 region amino acid sequences. Barcodes with two TCR α and two TCR β , or with three or more TCR α or TCR β chains were removed from further analyses using a custom R function built on the combine TCR function in the R package scRepertoire (v.1.8.0)⁸². Then, TCR clonotypes were integrated into scRNA-seq data using cell barcodes and were ordered by patient-specific clonal expansion. Overall, 74,865 T cells in tumour samples had paired single-cell RNA and TCR clonotype data.

We inferred the tumour or viral specificity of infiltrating T cells using previously defined gene expression signatures²⁸. Module scores were calculated for each tumour T cell with normalized RNA data using the Seurat function AddModuleScore. Scores were calculated for both the tumour-specific (TS) T cell gene signature and a virus-specific (VS) T cell gene signature. The gene sets were composed of upregulated genes with log₂ fold change above 1 from experimentally validated TS or VS CD8⁺ tumour-infiltrating lymphocytes, respectively. The module scores were used to quantify the enrichment of genes from a given gene signature in each cell. The gene signature score of each TCR clonotype was then determined by averaging the TS and VS signature score for each T cell in their clonotype. The density distribution of individual T cells and TCR clonotypes across TS and VS was assessed and, based on the dominating VS of normal T cells compared with tumour T cells and the near mutually exclusive distribution of TS and VS signature scores across TCR clonotypes, score thresholds were defined to infer the specificities of individual T cells and TCR clonotypes. Putative TS T cells and TCR clonotypes had TS scores greater than 0 and VS scores less than 0. Putative VS T cells and TCR clonotypes had VS scores greater than 0 and TS scores less than 0. Overall, the signature score threshold inferred 2,581 TS and 1,328 VS TCR clonotypes and comprised 37,007 and 5,650 inferred TS and VS T cells, respectively. Furthermore, for each TS and VS TCR clonotype, the percentage of cells with the same specificity as their clonotype was calculated. An average of 76.6% and 71% of cells were inferred to be TS across TS clonotypes and VS across VS clonotypes, respectively, according to the signature score thresholds described above. TS and VS clonotypes were filtered to retain those composed of 75% or more of TS cells or VS cells, respectively. Following this additional filtering, there were 1,635 TS and 270 VS TCR clonotypes. Finally, TS TCR clonotypes were further filtered by those clonotypes with expansion in both normal and tumour tissue to exclude non-tumour-specific clonotypes. TCR singletons and doubletons were

excluded from further analyses. Final inclusion parameters consisted of TS TCR clonotypes seen in tumours at a count between three and five and not seen in normal cells. For clonotypes seen in tumour above five counts, the count in normal cells must have been at least five cells fewer.

TCR-seq of peripheral blood T cells

Bulk sequencing of TCR β chains from peripheral T cells (PBMC samples) was performed as previously described^{28,83}. Raw data were processed using MiXCR (v.4.4.2)⁸⁴ and aligned using the built-in reference annotation (repseqio.v3.0.1) using the 'generic-amplicon-with-umi' preset, with the following additional parameters (--export-productive-clones-only --rna-tag-pattern '(R1:*)(UMI:N⁸⁵)(R2:*)' -Massemble.consensusAssemblerParameters=null -Massemble.cloneAssemblerParameters.addReadsCountOnClustering=true --floating-left-alignment-boundary --floating-right-alignment-boundary C). From the list of observed clonotypes for each technical replicate, we ran the exportClonesOverlap function with the following parameters (-tagCounts -vGene -jGene --criteria "CDR3|AA|V|J") to cluster all clonotypes with identical CDR3 amino acid sequence, variable (V) genes and joining (J) genes to generate consensus clonotypes for each biological sample. To further aggregate clonotypes, we merged TRBV genes (*TRBV6-2*, *TRBV6-3*, *TRBV6-5* and *TRBV6-6*; *TRBV12-3* and *TRBV12-4*) that are indistinguishable based on the locations of the RNase H-dependent PCR-enabled TCR-seq (rhTCR-seq) primers, as previously described⁸³. We then removed all UMIs supported by only one read and removed clones with no remaining UMIs. Clonotypes in a given sample with identical J genes and CDR3 amino acid sequences were then collapsed into the clonotype with the highest UMI count. Last, a report file was generated with aggregated UMI counts for each clonotype and the total number of unique clonotypes identified. These post-processing steps were written in Python and available at GitHub (https://github.com/Wu-Lab-DFCI-Harvard/bulkrhTCR_Script).

Four replicates were sequenced for each timepoint. In brief, CD3⁺ T cells were immunomagnetically isolated from thawed PBMCs samples (using anti-CD3 microbeads; Miltenyi), RNA was isolated (Qiagen) and rhTCR-seq was performed. This method uses RNase H-dependent PCR to enhance the specificity of TCR amplification and incorporates UMIs to each cDNA molecule to improve the accuracy of clonotype frequency estimations. Sequencing was performed on an Illumina MiSeq or a NextSeq 1000, and then MiXCR⁸⁴ was used to assemble TCR β clonotypes.

Inference of tumour specificity, viral specificity and vaccine specificity in peripheral blood T cells

The proportion of TS and VS T cells in the periphery was determined by matching clonotypes from the scTCR-seq analysis and the bulk TCR analysis. For each patient, the scTCR clonotypes were linked to bulk TCR clonotypes by matching the TCR β V gene, J gene and the CDR3 β amino acid sequence. The β -chains were separated for scTCR clonotypes with two identified β -chains. Owing to the high granularity of scTCR, multiple scTCR clonotypes were discovered to have the same β -chain identity but different α -chain identities. For each patient, an average (across all patients) of 19.9 TS clonotypes and 3.7 VS clonotypes had shared β -chains but unique α -chains. However, no β -chains were shared between TS and VS scTCR clonotypes. This matching process identified the inferred TS and VS TCR clonotypes in the peripheral T cells. For each patient and each timepoint, the frequencies of all inferred TS TCRs separately all inferred VS TCRs were reported for each individual patient at each timepoint. The arithmetic mean (and s.e.m.) and frequency of inferred TS and VS TCRs was graphed across all timepoints.

To infer the peripheral TCR clonotypes with vaccine-specificity, we identified TCR clonotypes that were either absent or just at the lower limit of detection in the pre-vaccination (week 0) sample, and then expanded by at least 10-fold in all of the subsequent timepoints

Article

(and having at least 3 UMI sequencing reads at ≥ 2 timepoints). For TCR clonotypes that were undetectable, their value was set to the nearest order of magnitude less than the smallest observed TCR frequency (that is, lower limit of detection) for that patient (10^{-4} for all patients). To increase stringency, we further required that these clonotypes be present in the scTCR analysis of the cutaneous DTH assessment (at week 13). The percentage frequency of all vaccine-inferred clonotypes were reported for each patient at each timepoint, and the arithmetic mean (and s.e.m.) of the percentage frequency of inferred vaccine-specific TCRs was graphed across all timepoints. For visualization in Fig. 4d and Extended Data Fig. 8b,c, later timepoints (collected past the 24-week protocol-mandated timepoints), TCR measurements were binned and displayed at the middle timepoint of the interval (weeks 50–74 were grouped and displayed at week 62, weeks 75–99 were grouped and displayed at week 87, weeks 100–124 were grouped and displayed at week 112, weeks 125–149 were grouped and displayed at week 137, and weeks 150–174 were grouped and displayed at week 162).

To infer whether each expanded clonotype consisted of CD4 or CD8 T cells, we traced clonotypes to single cells using the TCR β chain and integrated two complementary approaches for clonotype annotation. First, we used the paired scRNA-seq and TCR data from the skin (DTH assessment at week 13) to classify the T cell clonotypes as CD4 or CD8. Specifically, we used our per cluster annotation (as defined in Fig. 3 and Extended Data Fig. 9a,b). Next, we used a per cell annotation through reference mapping to a human CD4 (<https://doi.org/10.6084/m9.figshare.21981536.v1>) and CD8 atlas (<https://doi.org/10.6084/m9.figshare.23608308.v1>) with the tool ProjectTILs (v.3.3.1)⁸⁶. The majority of clonotypes (53 out of 98) had concordant phenotype annotations by both methods, defined by >75% of their cells being classified as CD4 or CD8. An additional 25 clonotypes were annotated as CD4 or CD8 by only one of the methods given an unresolved annotation by the second method. For 11 clonotypes that had discordant CD4 versus CD8 annotation by the 2 methods, the expression of *CD4* and *CD8A* were manually evaluated and cells were annotated on the basis of the unique detection of one of these genes, which resulted in an additional 3 clones annotated as CD4 or CD8. We additionally excluded one cell as its matching TCR clonotype comprised two β -chains, thus we could not unambiguously match the clonotypes observed in the (unpaired) bulk TCR data. The remaining cells remained as unresolved (that is, could not confidently annotated as CD4 or CD8).

Statistics and reproducibility

Given the limited primary patient material, experiments were typically performed a single time (when appropriate, technical replicates were performed during that experiment). In limited cases (specifically for IFN γ ELISpot assays), experiments may have been repeated if there was a failure of positive or negative controls and there was sufficient primary patient material to repeat the experiment.

Reporting summary

Further information on research design is available in the Nature Portfolio Reporting Summary linked to this article.

Data availability

The list of somatic mutations for all patients (mutation annotation file) is available in Supplementary Table 1. The IFN γ ELISpot responses for ex vivo peptide pool stimulation, in vitro individual peptide stimulation and autologous tumour testing are available in Supplementary Table 2. The median normalized protein expression (NPX) values of circulating soluble proteins is available in Supplementary Table 3. The cell numbers and T cell clonotype metrics from scRNA-seq and TCR-seq of skin samples are available in Supplementary Table 4. The T cell clonotype metrics for tumour-infiltrating T cells and for peripheral T cells are

available in Supplementary Table 5. The individual T cell clonotypes and their corresponding phenotypes are available in Supplementary Table 6. The reference genome (hg19) and transcriptome (GENCODE v.19) are publicly available online through Google Cloud Storage (<https://firecloud-tcga-open-access/tutorial/reference/annotation.db.ucsc.hg19.tar> and https://firecloud-tcga-open-access/tutorial/reference/rna-seq/gencode.v19.genes.v7_model.patched_contigs.gtf, respectively). All raw DNA and RNA sequencing files for the tumour samples have been deposited into dbGaP (phs003710.v1.p1). Source data are provided with this paper.

Code availability

The algorithms used for data analyses are all publicly available from in the indicated references in the Methods. For the bulk TCR processing pipeline, the code is available at GitHub (https://github.com/Wu-Lab-DFCI-Harvard/bulkrhTCR_Script).

58. Liu, N., Zhou, Y. & Lee, J. J. IPDfromKM: reconstruct individual patient data from published Kaplan–Meier survival curves. *BMC Med. Res. Methodol.* **21**, 111 (2021).
59. Fisher, S. et al. A scalable, fully automated process for construction of sequence-ready human exome targeted capture libraries. *Genome Biol.* **12**, R1 (2011).
60. Huang, C. et al. Proteogenomic insights into the biology and treatment of HPV-negative head and neck squamous cell carcinoma. *Cancer Cell* **39**, 361–379 (2021).
61. Taylor-Weiner, A. et al. DeTIN: overcoming tumor-in-normal contamination. *Nat. Methods* **15**, 531–534 (2018).
62. Cibulskis, K. et al. ContEst: estimating cross-contamination of human samples in next-generation sequencing data. *Bioinformatics* **27**, 2601–2602 (2011).
63. Kent, W. J. BLAT—the BLAST-like alignment tool. *Genome Res.* **12**, 656–664 (2002).
64. Cibulskis, K. et al. Sensitive detection of somatic point mutations in impure and heterogeneous cancer samples. *Nat. Biotechnol.* **31**, 213–219 (2013).
65. Saunders, C. T. et al. Strelka: accurate somatic small-variant calling from sequenced tumor–normal sample pairs. *Bioinformatics* **28**, 1811–1817 (2012).
66. Ramos, A. H. et al. Oncotator: cancer variant annotation tool. *Hum. Mutat.* **36**, E2423–E2429 (2015).
67. Carter, S. L. et al. Absolute quantification of somatic DNA alterations in human cancer. *Nat. Biotechnol.* **30**, 413–421 (2012).
68. Dobin, A. et al. STAR: ultrafast universal RNA-seq aligner. *Bioinformatics* **29**, 15–21 (2013).
69. Li, B. & Dewey, C. N. RSEM: accurate transcript quantification from RNA-seq data with or without a reference genome. *BMC Bioinform.* **12**, 323 (2011).
70. DeLuca, D. S. et al. RNA-SeQC: RNA-seq metrics for quality control and process optimization. *Bioinformatics* **28**, 1530–1532 (2012).
71. Sarkizova, S. et al. A large peptidome dataset improves HLA class I epitope prediction across most of the human population. *Nat. Biotechnol.* **38**, 199–209 (2020).
72. Jurtz, V. et al. NetMHCpan-4.0: improved peptide–MHC class I interaction predictions integrating eluted ligand and peptide binding affinity data. *J. Immunol.* **199**, 3360–3368 (2017).
73. Lawrence, M. S. et al. Discovery and saturation analysis of cancer genes across 21 tumour types. *Nature* **505**, 495–501 (2014).
74. Lee, P. C. et al. Reversal of viral and epigenetic HLA class I repression in Merkel cell carcinoma. *J. Clin. Invest.* **132**, e151666 (2022).
75. Keskin, D. B. et al. Direct identification of an HPV-16 tumor antigen from cervical cancer biopsy specimens. *Front. Immunol.* **2**, 75 (2011).
76. Hao, Y. et al. Integrated analysis of multimodal single-cell data. *Cell* **184**, 3573–3587 (2021).
77. McGinnis, C. S., Murrow, L. M. & Gartner, Z. J. DoubletFinder: doublet detection in single-cell RNA sequencing data using artificial nearest neighbors. *Cell Syst.* **8**, 329–337 (2019).
78. Germain, P. L., Lun, A., Garcia Meixide, C., Macnair, W. & Robinson, M. D. Doublet identification in single-cell sequencing data using scDblFinder. *F1000Research* **10**, 979 (2021).
79. Korsunsky, I. et al. Fast, sensitive and accurate integration of single-cell data with Harmony. *Nat. Methods* **16**, 1289–1296 (2019).
80. Zappia, L. & Oshlack, A. Clustering trees: a visualization for evaluating clusterings at multiple resolutions. *Gigascience* **7**, gty083 (2018).
81. Street, K., Movassagh, M. & Lundell, J. VDJdive: analysis tools for 10X V(D)J data. R package v.1.3.5. *Bioconductor* <https://www.bioconductor.org/packages/release/bioc/html/VJDive.html> (2024).
82. Borchertding, N., Bormann, N. L. & Kraus, G. scRepertoire: an R-based toolkit for single-cell immune receptor analysis. *F1000Research* **9**, 47 (2020).
83. Li, S. et al. RNase H-dependent PCR-enabled T-cell receptor sequencing for highly specific and efficient targeted sequencing of T-cell receptor mRNA for single-cell and repertoire analysis. *Nat. Protoc.* **14**, 2571–2594 (2019).
84. Bolotin, D. A. et al. MiXCR: software for comprehensive adaptive immunity profiling. *Nat. Methods* **12**, 380–381 (2015).
85. Abelin, J. G. et al. Mass spectrometry profiling of HLA-associated peptidomes in mono-allelic cells enables more accurate epitope prediction. *Immunity* **46**, 315–326 (2017).
86. Andreatta, M. et al. Interpretation of T cell states from single-cell transcriptomics data using reference atlases. *Nat. Commun.* **12**, 2965 (2021).

Acknowledgements We thank M. Harden for her assistance in coordinating tissue transfer for sequencing and J. Tsuji for assistance with genomic analyses; M. Sellars and L. Pomerance for input on immune analyses and R. Shear for assistance with data deposition; staff at Almac Sciences for the manufacture of vaccine peptides and staff at Bristol-Myers Squibb for providing ipilimumab. This work is supported in part by a grant from the Gateway for Cancer Research and the Department of Defense CDMRP Kidney Cancer Research Program (KC190130). D.A.B. acknowledges support from the Department of Defense Early Career Investigator grant (KCRP AKCI-ECI, W81XWH-20-1-0882), the Louis Goodman and Alfred Gilman Yale Scholar Fund, the NIH/NCI (1R37CA279822-01) and the Yale Cancer Center (supported by NIH/NCI research grant P30CA016359). E.B. received support from the Dana-Farber Cancer Immunology Training Program (NIH T32CA207021). S.L. is supported by the NCI Research Specialist Award (R50CA251956). J.B.I. acknowledges support from the National Institutes of Health (K12CA090354) and Conquer Cancer Foundation/Sontag Foundation. S.K. is currently an employee of Genentech. G.O. was supported by the Claudia Adams Barr Program for Innovative Cancer Research and by DF/HCC Kidney Cancer SPORE P50 CA101942. S.A.S. is supported by the Cancer Prevention and Research Institute of Texas (CPRIT) award RR220009. This work was supported in part by grants P01CA206978 to S.A.C. from the NIH, U24CA270823 and U01CA271402 to S.A.C. from the National Cancer Institute (NCI) Clinical Proteomic Tumour Analysis Consortium programme, as well as a grant from the Dr. Miriam and Sheldon G. Adelson Medical Research Foundation to S.A.C. C.J.W. acknowledges support by DF/HCC Kidney Cancer SPORE P50 CA101942. D.B.K. is supported by the NHLBI 1R01HL157174-01A1. P.A.O. is supported in part by NCI-1R01CA229261, the Francis and Adele Kittredge Family Immuno-Oncology and Melanoma Research Fund, the Fisher Family Fund, The Morgan Family Fund for Melanoma Research, the Susana and Bruce Hampton Research Fund and the Faircloth Family Research Fund. T.K.C. is supported in part by the Dana-Farber Harvard Cancer Center Kidney SPORE (2P50CA010942-16) and Program 5P30CA006516-56, the Kohlberg Chair at Harvard Medical School and the Trust Family, Michael Brigham, Pan Mass Challenge, Hinda and Arthur Marcus Fund, and Loker Pinard Funds for Kidney Cancer Research at DFCl. The funders had no role in the conduct of the trial or in the analysis of clinical or immunological end points.

Author contributions D.A.B. contributed to the conception and design of the work, acquisition, analysis and interpretation of data and drafted the manuscript. G.M., V.C., B.A.M., E.B., C.R.T., A.P.V., C.F., J.F., A.B.A., N.R.S., S.L., J.S., S.L.C., M.S.H., N.R.L., O.O., A.M., H.G., K.S., S.K., S. Sarkizova, C.B.P., M.M., I.C., A.T., J.D.-C., A.A.H., J.B.I., S. Signoretti, J.C.A., L.E., S.A.C., I.L., G.G., S.G., N.H., L.R.O., G.O., D.S.N., K.J.L. and S.A.S. contributed to the analysis and interpretation of data and substantial revision to the manuscript. Y.L. contributed to the analysis of data and substantial revision to the manuscript. B.S. and J.M.S. contributed to the analysis of data, creation of new software used in the work and substantial revision to the manuscript. E.F.F., C.J.W., D.B.K., P.A.O. and T.K.C. contributed to the initial conception and design of the work, analysis and interpretation of data and substantial revision to the manuscript. The authors assume responsibility for the completeness and accuracy of the data.

Competing interests Bristol-Myers Squibb provided ipilimumab, but no funding support for the clinical trial. D.A.B. reports share options in Elephas; advisory board, consulting or personal fees from Cancer Expert Now, Adnovate Strategies, MDedge, CancerNetwork, Catenion, OncLive, Cello Health BioConsulting, PWW Consulting, Haymarket Medical Network, Aptitude Health, ASCO Post and Harborside, Targeted Oncology, Merck, Pfizer, MedScape, Accolade 2nd MD, DLA Piper, AbbVie, Compugen, Link Cell Therapies, Scholar Rock, NeoMorph, Nimbus, Exelixis, AVEO, Eisai and Elephas; and research support from Exelixis and AstraZeneca, outside the submitted work. B.A.M. discloses personal consulting fees from Arcus, Aveo, Bristol-Myers Squibb, Daiichi Sanko, Eisai, Exelixis, Genmab, Gilead, Hexagen, Pfizer and SeaGen, and institutional disclosures for Aveo, Bristol-Myers Squibb, Exelixis, Gilead, Pfizer and SeaGen. N.R.L. is a consultant and has received honoraria from Bayer, Seattle Genetics, Sanofi, Silverback, Fortress Biotech, Synox Therapeutics, Janssen and Astellas pharma, outside the submitted work. K.S. is now an employee and shareholder of Intellia Therapeutics, which has no contribution or affiliation to the work described in this article. S.K. is now an employee of Genentech. S. Sarkizova is now an employee of Moderna and holds stock (as of January 2024). J.B.I. reports receiving consulting fees from AstraZeneca outside the submitted work. S. Signoretti reports receiving commercial research grants from Bristol-Myers Squibb, AstraZeneca, Exelixis, Merck, NiKang Therapeutics and Arsenal Biosciences; is a consultant/advisory board member for Merck, AstraZeneca, Bristol Myers Squibb, CRISPR Therapeutics AG, AACR and NCI; receives royalties from Biogenex; and mentored several non-United States citizens on research projects with

potential funding (in part) from non-United States sources/Foreign Components. J.C.A. has served as a consultant for Remix Therapeutics, Ayala Pharmaceuticals, Cellestia, and on the scientific advisory board of NeuAPC, outside the submitted work. S.A.C. is a member of the scientific advisory boards of PTM BioLabs, Seer, StandUp2Cancer and PrognomiQ. I.L. serves as a consultant for PACT Pharma and has stock, is on the board and serves as a consultant for ennovi, and is on the board and holds equity in Nord Bio. G.G. receives research funds from IBM, Pharmacyclics/Abbvie, Bayer, Genentech, Calico, Ultima Genomics, Inocras and Google and is also an inventor on patent applications filed by the Broad Institute related to MSMuTect, MSMutSig, POLYSOLVER, SignatureAnalyzer-GPU, MSeYE and MinimuMM-seq. He is a founder, consultant and holds privately held equity in Scorpion Therapeutics; he is also a founder of, and holds privately held equity in, PreDICTA Biosciences. He was also a consultant to Merck. N.H. holds equity in and advises Danger Bio/Related Sciences and Repertoire Immune Medicines, owns equity in BioNtech and receives research funding from Bristol Myers Squibb and Calico Life Sciences. D.S.N. owns stock in Madrigal Pharmaceuticals, outside the submitted work. K.J.L. holds equity in Standard BioTools and is on the scientific advisory board for MBQ Pharma. S.A.S. reports equity in Agenus, Agios Pharmaceuticals, Breakbio, Bristol-Myers Squibb and Lumos Pharma. S.A.S. is a consultant for Imunon and Jivanu therapeutics. E.F.F. is an equity holder in and consultant for BioNTech, an equity holder and scientific advisory board member of BioEntre, and a founder and equity holder of Dionis Therapeutics. C.J.W. is subject to a conflict-of-interest management plan for the reported studies because of her former competing financial interests in Neon Therapeutics, which was acquired by BioNTech. Under this plan, C.J.W. may not access identifiable data for human participants or otherwise participate directly in the Institutional Review Board-approved protocol reported herein. C.J.W.'s contributions to the overall strategy and data analyses occurred on a de-identified basis. Patent applications have been filed on aspects of the described work entitled as follows: 'Compositions and methods for personalized neoplasia vaccines' (N.H., E.F.F. and C.J.W.), 'Methods for identifying tumour specific neoantigens' (N.H. and C.J.W.), 'Formulations for neoplasia vaccines' (E.F.F.) and 'Combination therapy for neoantigen vaccine' (N.H., C.J.W. and E.F.F.). The DFCl, the lead site of this trial, has a proprietary and financial interest in the personalized neoantigen vaccine. D.B.K. is a scientific advisor for Immunitrack, a wholly owned subsidiary of Eli Lilly and Company and Breakbio. D.B.K. owns equity in Affimed N.V., Agenus, Armata Pharmaceuticals, Breakbio, BioMarin Pharmaceuticals, Celldex Therapeutics, Editas Medicine, Immunitybio, Lexicon Pharmaceuticals, Summit Therapeutics and Viking Therapeutics. P.A.O. has received research funding from and/or has advised Agenus, Amgen, Armo BioSciences Array, AstraZeneca/MedImmune, Bristol-Myers Squibb, Celldex, Compass Therapeutics, CytomX, Evaxion, Immunetune, Imunon, LGChem, Merck, Neon Therapeutics (now BioNTechUS), Novartis, Pharmajet, Phio, Pfizer, Oncorus, Roche/Genentech, Servier and Xencor. Committees: NCCN. T.K.C. reports grants, personal fees and non-financial support from Roche and Genentech during the conduct of the study; and reports institutional and/or personal, paid and/or unpaid support for research, advisory boards, consultancy, and/or honoraria from Alkermes, AstraZeneca, Aravive, Aveo, Bayer, Bristol Myers-Squibb, Calithera, Circle Pharma, Eisai, EMD Serono, Exelixis, GlaxoSmithKline, Gilead, IQVA, Infinity, Ipsen, Jansen, Kanaph, Lilly, Merck, Nikang, Nuscan, Novartis, Oncohost, Pfizer, Roche, Sanofi/Aventis, Scholar Rock, Surface Oncology, Takeda, Tempest, Up-To-Date, CME events (Peerview, OncLive, MJH and others), outside the submitted work. Institutional patents filed on molecular alterations and immunotherapy response/toxicity, and ctDNA. Equity: Tempest, Pionyr, Osel, Precede Bio, CureResponse, InnDura Therapeutics, Primium. Committees: NCCN, GU Steering Committee, ASCO/ESMO, ACCRU, KidneyCan, ODAC. Mentored several non-United States citizens on research projects with potential funding (in part) from non-United States sources/Foreign Components. The institution (Dana-Farber Cancer Institute) may have received additional independent funding of drug companies and/or royalties potentially involved in research around the subject matter. G.M., V.C., E.B., C.R.T., A.P.V., C.F., J.F., A.B.A., N.R.S., Y.L., S.L., J.S., S.L.C., M.S.H., O.O., A.M., H.G., C.B.P., M.M., I.C., A.T., J.D.-C., A.A.H., B.S., J.M.S., L.E., L.R.O., S.G. and G.O. have no reported disclosures related to the current work.

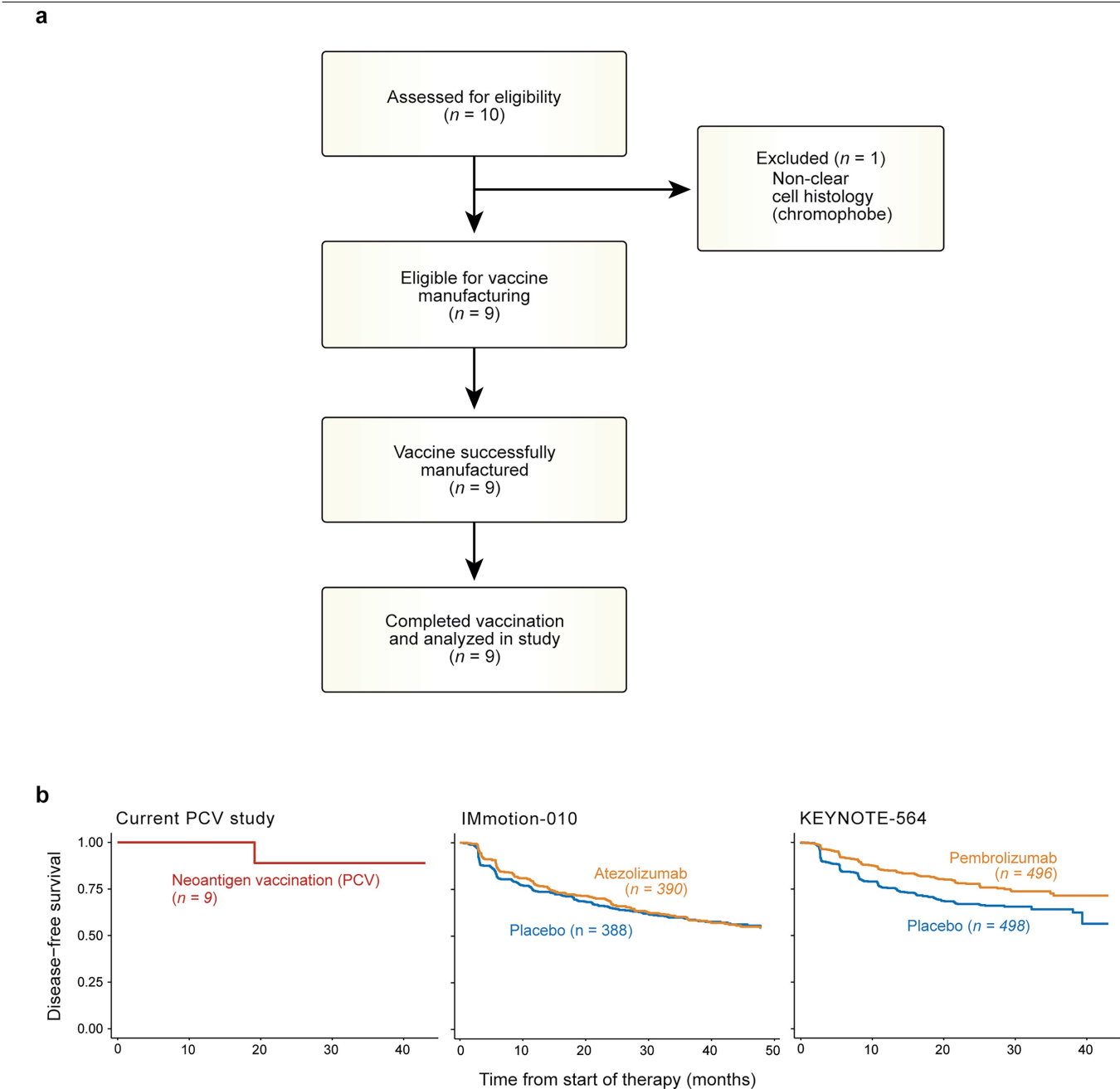
Additional information

Supplementary information The online version contains supplementary material available at <https://doi.org/10.1038/s41586-024-08507-5>.

Correspondence and requests for materials should be addressed to David A. Braun, Catherine J. Wu or Toni K. Choueiri.

Peer review information *Nature* thanks Cornelis Melief and the other, anonymous, reviewer(s) for their contribution to the peer review of this work.

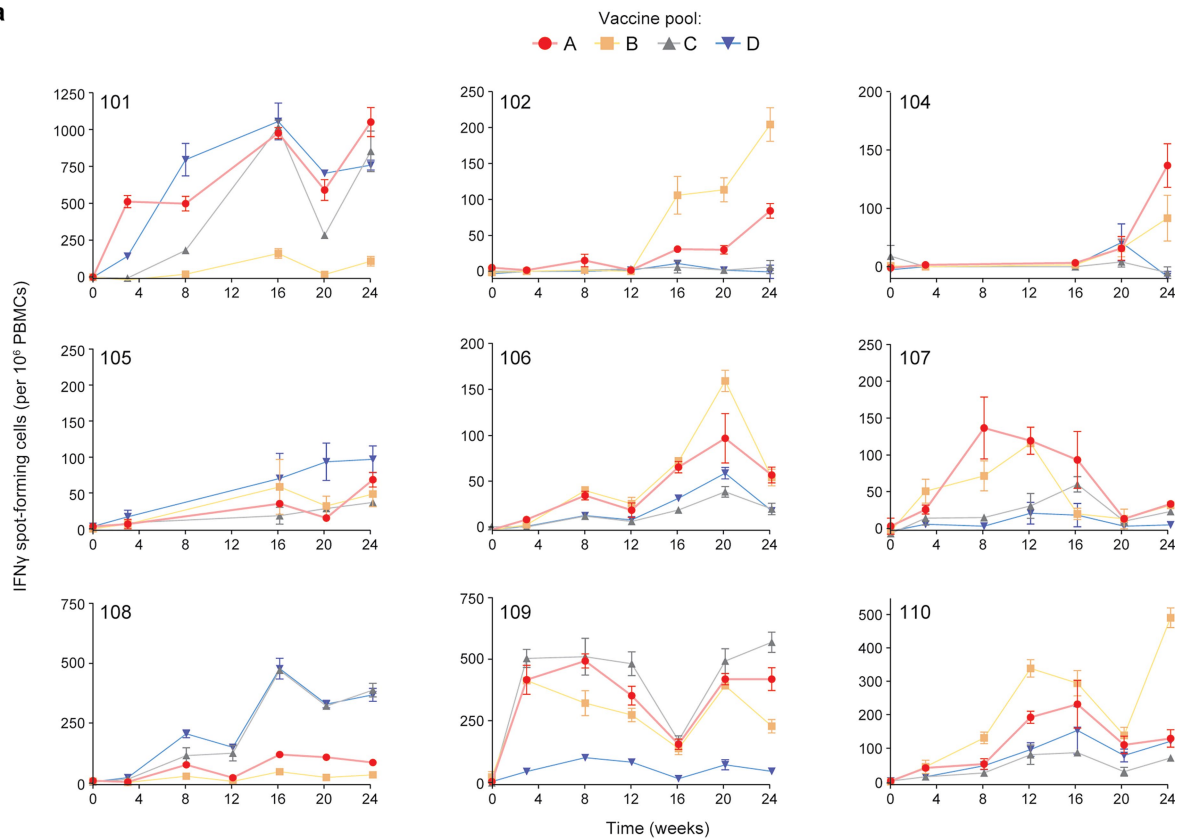
Reprints and permissions information is available at <http://www.nature.com/reprints>.



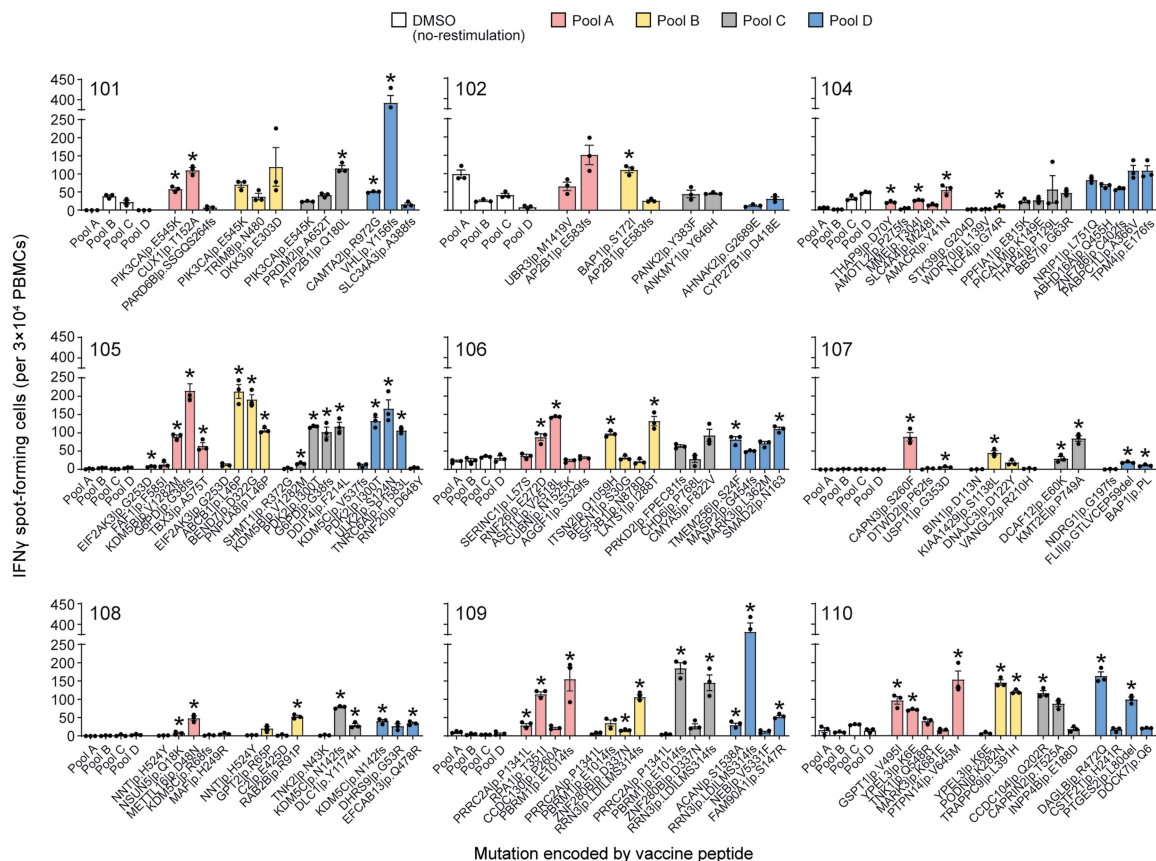
Extended Data Fig. 1 | Study description and qualitative comparison to modern RCC adjuvant trials. a, CONSORT diagram describing screening, enrollment, vaccine manufacturing, and treatment. b, Kaplan-Meier plots of disease-free survival from the current PCV study (*left*) and two recent,

randomize phase III adjuvant immune checkpoint inhibitor trials in RCC with similar eligibility criteria, (*middle*) the IMmotion-010 trial of atezolizumab vs placebo, and (*left*) the KEYNOTE-564 of pembrolizumab vs placebo.

a

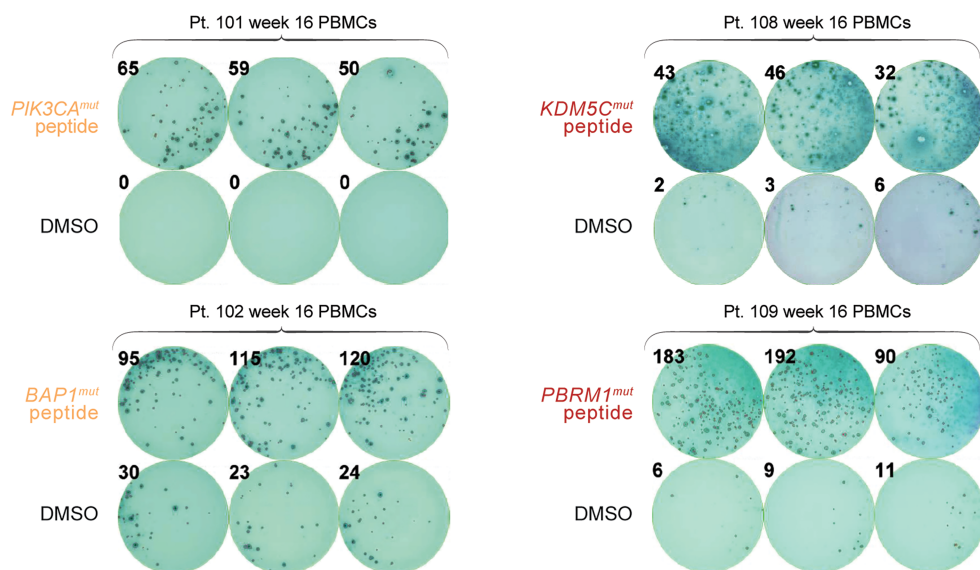
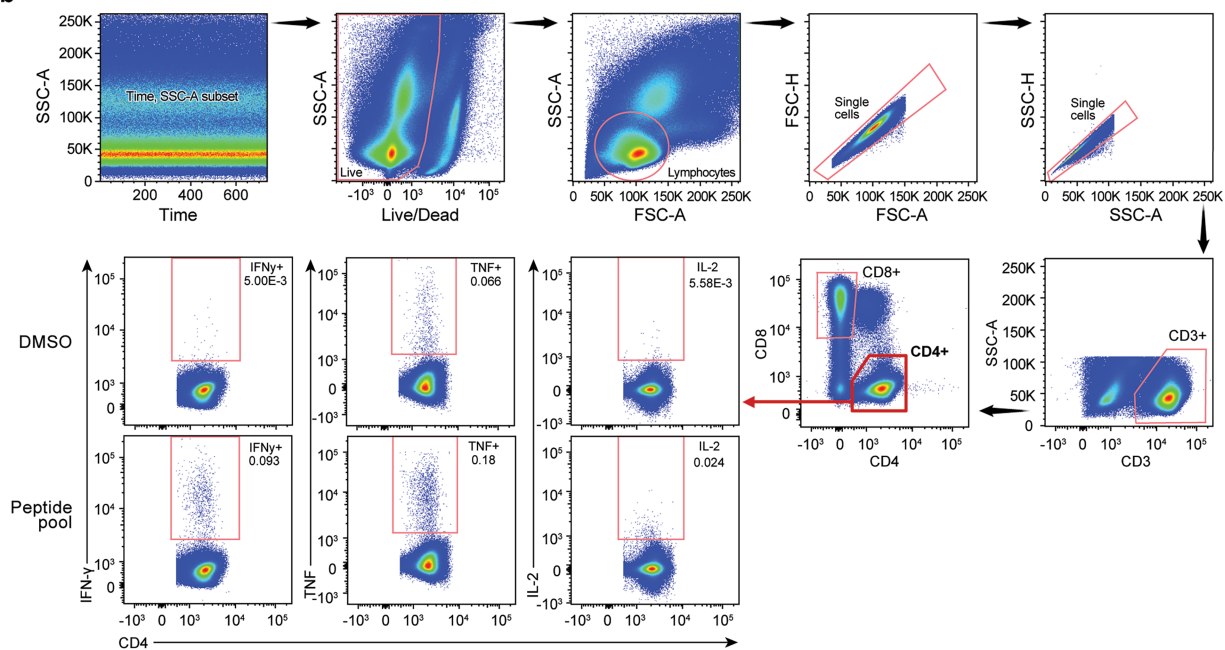
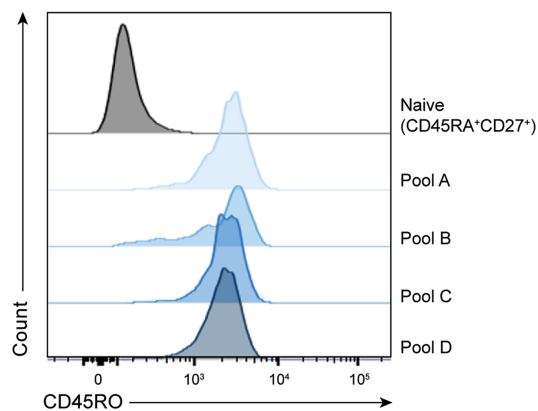
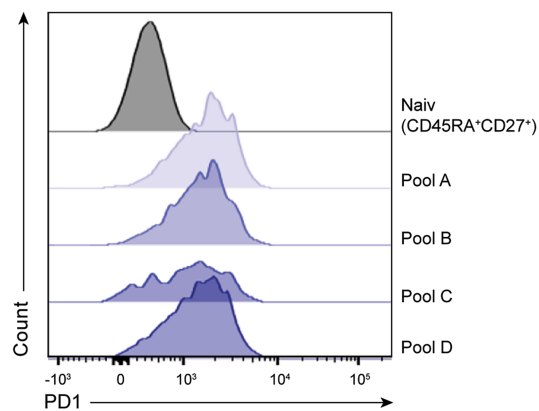


b

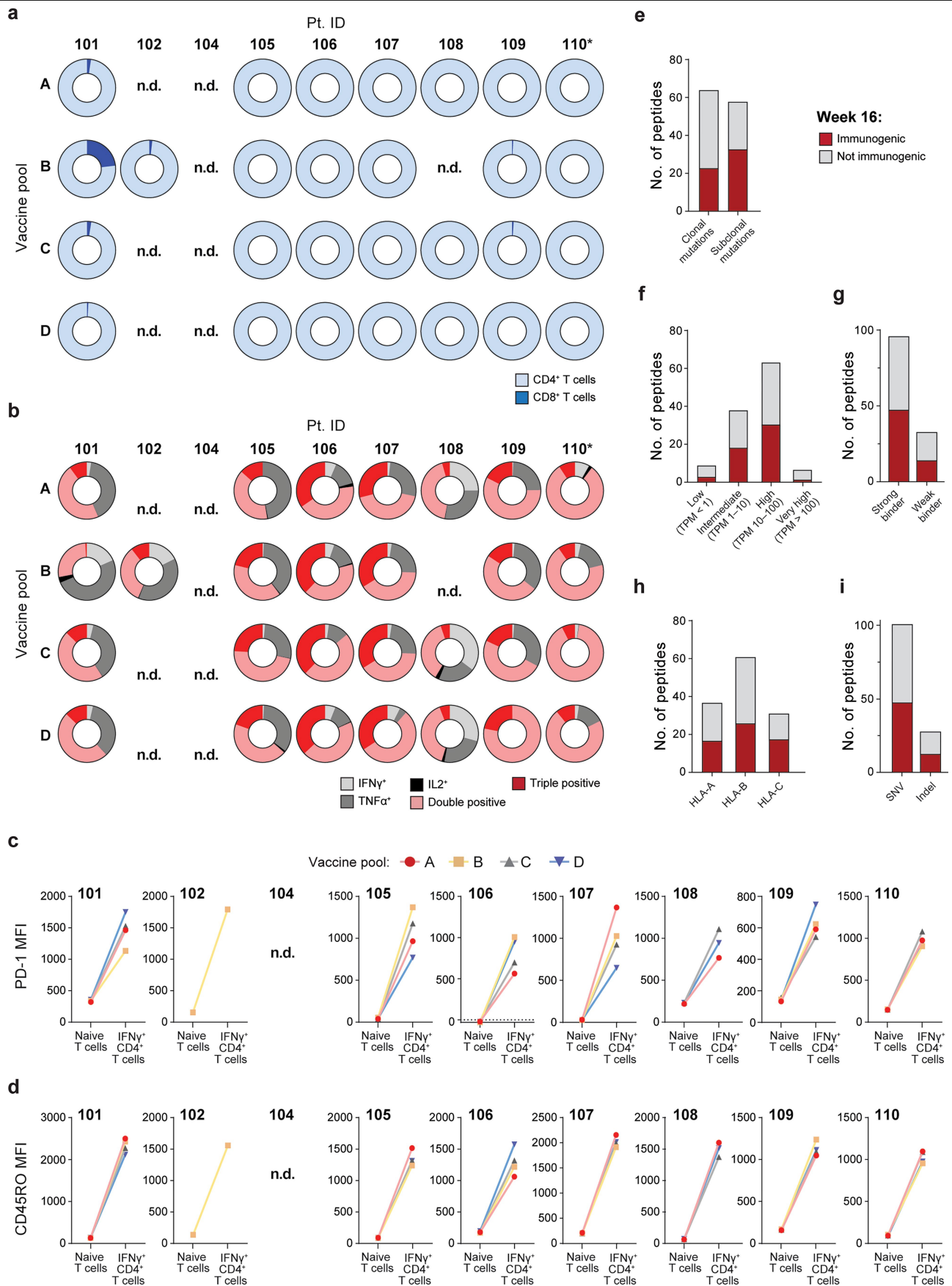


Extended Data Fig. 2 | See next page for caption.

Extended Data Fig. 2 | Peripheral T cell responses to vaccination. a, ex vivo dynamics of peripheral T cell response to vaccination. For each patient (101 through 110), the ex vivo PBMC IFN γ ELISpot response for each vaccine peptide pool at each timepoint following start of vaccination (week 0), normalized to 10^6 PBMCs. Each point is the background-subtracted mean of three replicates with standard error of the mean. b, deconvolution of individual neoantigen-containing vaccine peptides that generated T cell responses to vaccination. For each patient and each vaccine pool, week 16 PBMCs were stimulated in vitro with all peptides in that pool, rested, and then left unstimulated (DMSO) or re-stimulated with the individual mutation-encoding vaccine peptide. Each graph represents the absolute IFN γ ELISpot count (mean of triplicates with standard error of the mean; * indicates $P < 0.05$ by two-sided t-test and mean spot count at least three-fold higher than DMSO control).

a**b****c****d****Extended Data Fig. 3** | See next page for caption.

Extended Data Fig. 3 | Characterization of peripheral immune responses to vaccination. a, Example IFN γ ELISpots for selected driver mutations, including SNVs (*PIK3CA* and *BAP1*) and indels (*KDM5C* and *PBRM1*). b, Gating strategy for flow cytometry assessment of T cell cytokine production and phenotype. Example flow cytometry gating strategy for identifying CD4 $^{+}$ and CD8 $^{+}$ T cells, and production of IFN γ , TNF α , and IL-2 cytokines in those T cell subsets. c, Expression of CD45RO and, d, PD-1 on CD4 $^{+}$ IFN γ $^{+}$ (vaccine-reactive) T cells (as measured by the median fluorescence intensity; MFI) after stimulation with vaccine peptide pools.



Extended Data Fig. 4 | See next page for caption.

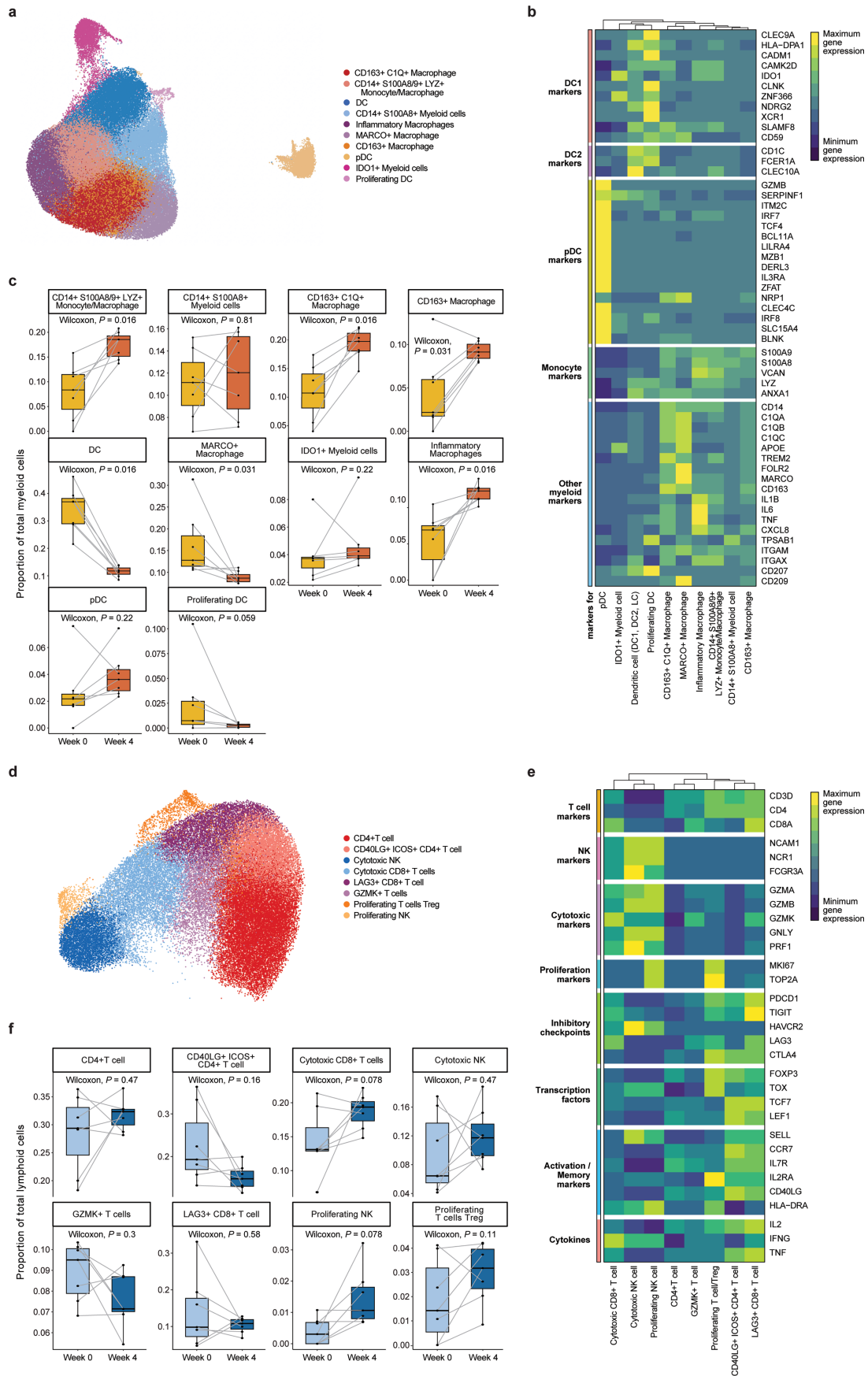
Extended Data Fig. 4 | Patient-level T cell immunophenotyping and intracellular cytokine production, and Impact of tumor-intrinsic and -extrinsic features on antigen immunogenicity. a, Per-patient CD4+ and CD8+ composition of vaccine-reactive (IFN γ +) T cells for each vaccine peptide pool and each patient (week 16 after vaccination). n.d., not detectable (the absolute number of IFN γ + cells were too low for evaluation, or the frequency of IFN γ was not at least 1.5-fold higher than the negative control, HIV gag protein). * The additional negative control, HIV gag, was not available for patient 110 analysis. The results are reported here for reference, but not included in the overall summary. b, Per-patient and per-vaccine pool assessment of cytokine production. For each patient, the median fluorescence intensity (MFI) of (c) PD-1 (d) CD45RO for vaccine-reactive (IFN γ +) CD4+ T cells compared to

naïve T cells (CD45RA+CD27+) is shown. e-i, the immunogenicity of each neoantigen-containing vaccine peptide was assessed by stimulation of week 16 PBMCs (in vitro stimulation) and measurement of IFN γ + by ELISpot. For tumor-intrinsic features, the immunogenicity of each vaccine peptide was examined based on (e) the clonality of the underlying mutation in the tumor and (f) the expression of that gene (measured in transcripts per million; TPM). For tumor-extrinsic features, the immunogenicity of each vaccine peptides was examined based on (g) whether the predicted T cell epitope was inferred as a strong (rank <0.5) or weak (rank <2) HLA class I binder, (h) which HLA class I allele the epitope was predicted to bind to, and (i) whether the neoantigen was derived from an SNV or an indel.



Extended Data Fig. 5 | Global changes in the circulating immune milieu following vaccination. Measurement of circulating (plasma) soluble proteins prior to vaccination (week 0), during vaccine priming (week 3), and 8 weeks after the first vaccine boost (week 20) for 92 circulating cytokines ($n=8$ patients

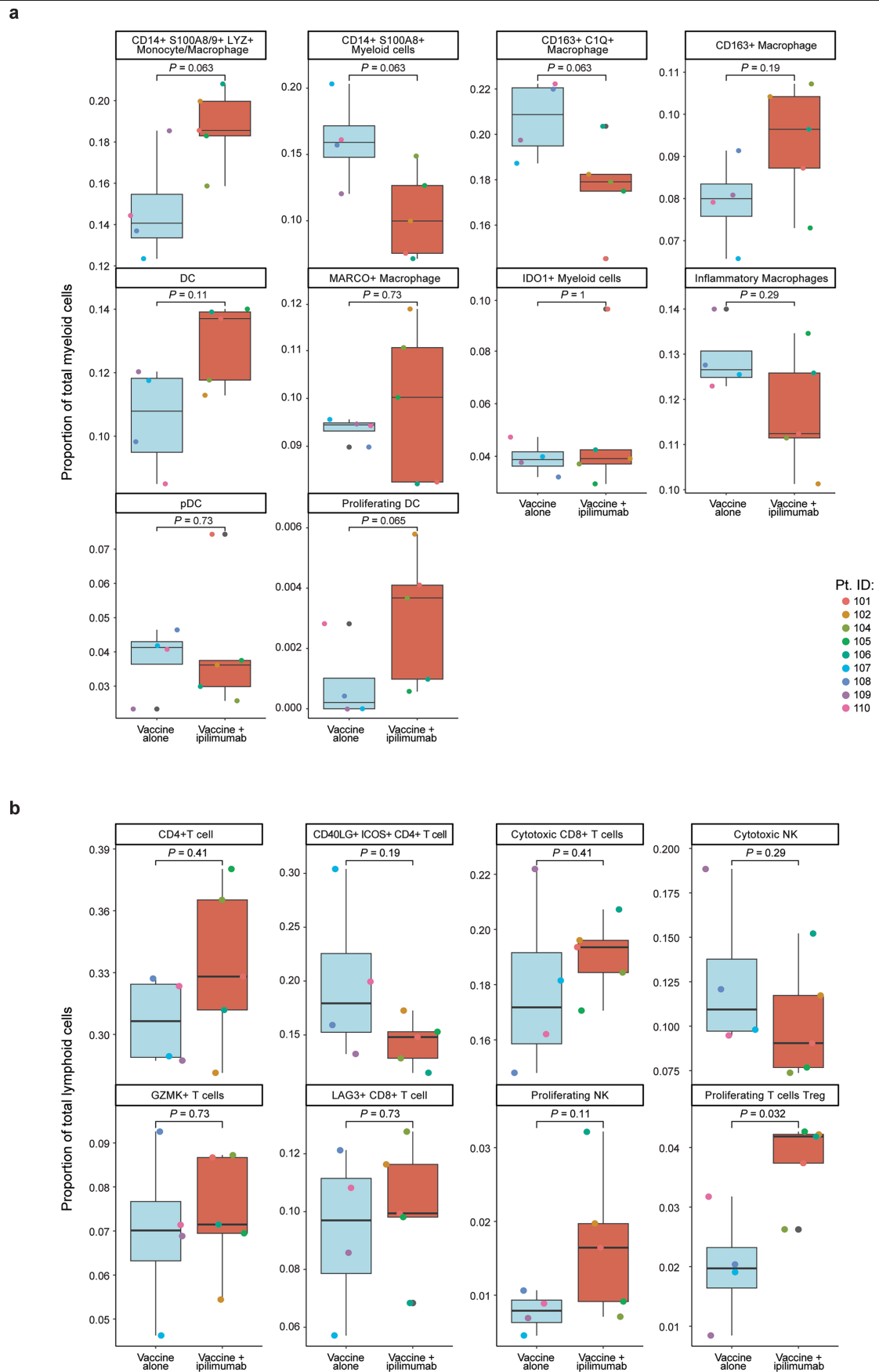
for week 0, $n=9$ patients for week 3, and $n=9$ patients for week 20; boxplot hinges represent 25th to 75th percentiles, central lines represent the medians, the whiskers extend to lowest and highest values no greater than $1.5 \times$ interquartile range away from the 25th and 75th percentiles, and the dots indicate outliers).



Extended Data Fig. 6 | See next page for caption.

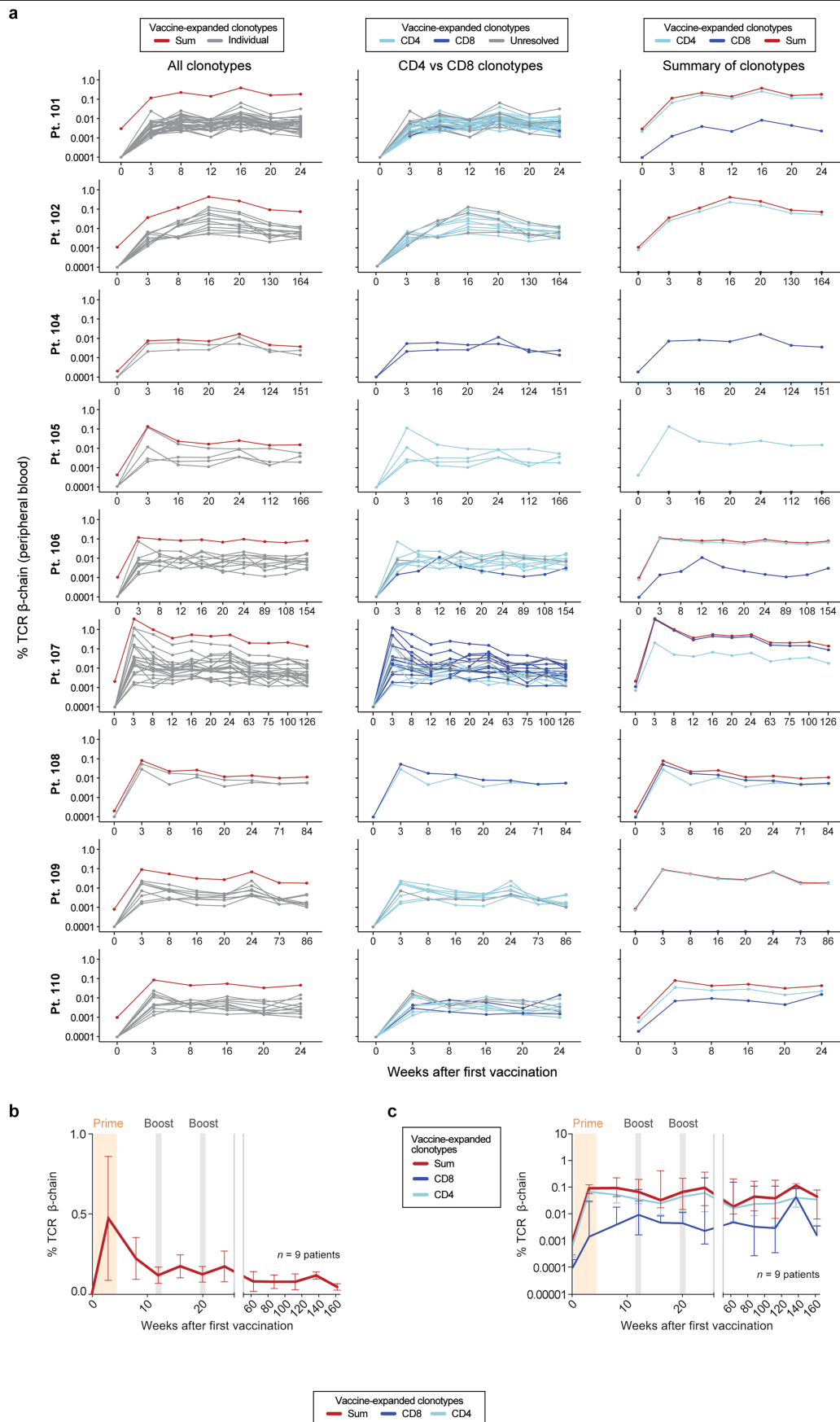
Extended Data Fig. 6 | Single-cell transcriptomic analysis of skin-infiltrating immune cells at the site of vaccination. a, UMAP representation of scRNA-seq of skin-infiltrating myeloid cells (N = 9 patients) at the vaccination site (right thigh). b, Heatmap of marker gene expression for each myeloid population, which was utilized to assign identity to each cell cluster. c, Boxplots of the proportion of each myeloid cell population before and after vaccination (two-sided paired Wilcoxon test; $n = 7$ paired samples, as $n = 2$ patients had insufficient material at baseline for scRNA-seq; boxplot hinges represent 25th to 75th percentiles, central lines represent the medians, the whiskers extend to lowest and highest values no greater than $1.5 \times$ interquartile range away from the 25th and 75th percentiles, and the dots indicate outliers). DC1: conventional dendritic cell (type 1); DC2: conventional dendritic cell (type 2);

pDC: plasmacytoid dendritic cell. LC: Langerhans cell. d, UMAP representation of scRNA-seq of skin-infiltrating lymphoid cells (N = 9 patients) at the vaccination site (right thigh). e, Heatmap of marker gene expression for each lymphoid population, which was utilized to assign identity to each cell cluster. f, Boxplots of the proportion of each lymphoid cell population before and after vaccination (two-sided paired Wilcoxon test; $n = 7$ paired samples, as $n = 2$ patients had insufficient material at baseline for scRNA-seq; boxplot hinges represent 25th to 75th percentiles, central lines represent the medians, the whiskers extend to lowest and highest values no greater than $1.5 \times$ interquartile range away from the 25th and 75th percentiles, and the dots indicate outliers). NK cell: natural killer cell.



Extended Data Fig. 7 | Minimal impact of subcutaneous ipilimumab on skin-infiltrating immune cells. The proportion of each (a) myeloid cell and (b) lymphoid cell population after vaccination (week 4) was compared in patients who received the vaccine alone or vaccine plus subcutaneous ipilimumab (two-sided Wilcoxon test; $n = 4$ patients who received vaccine alone, and

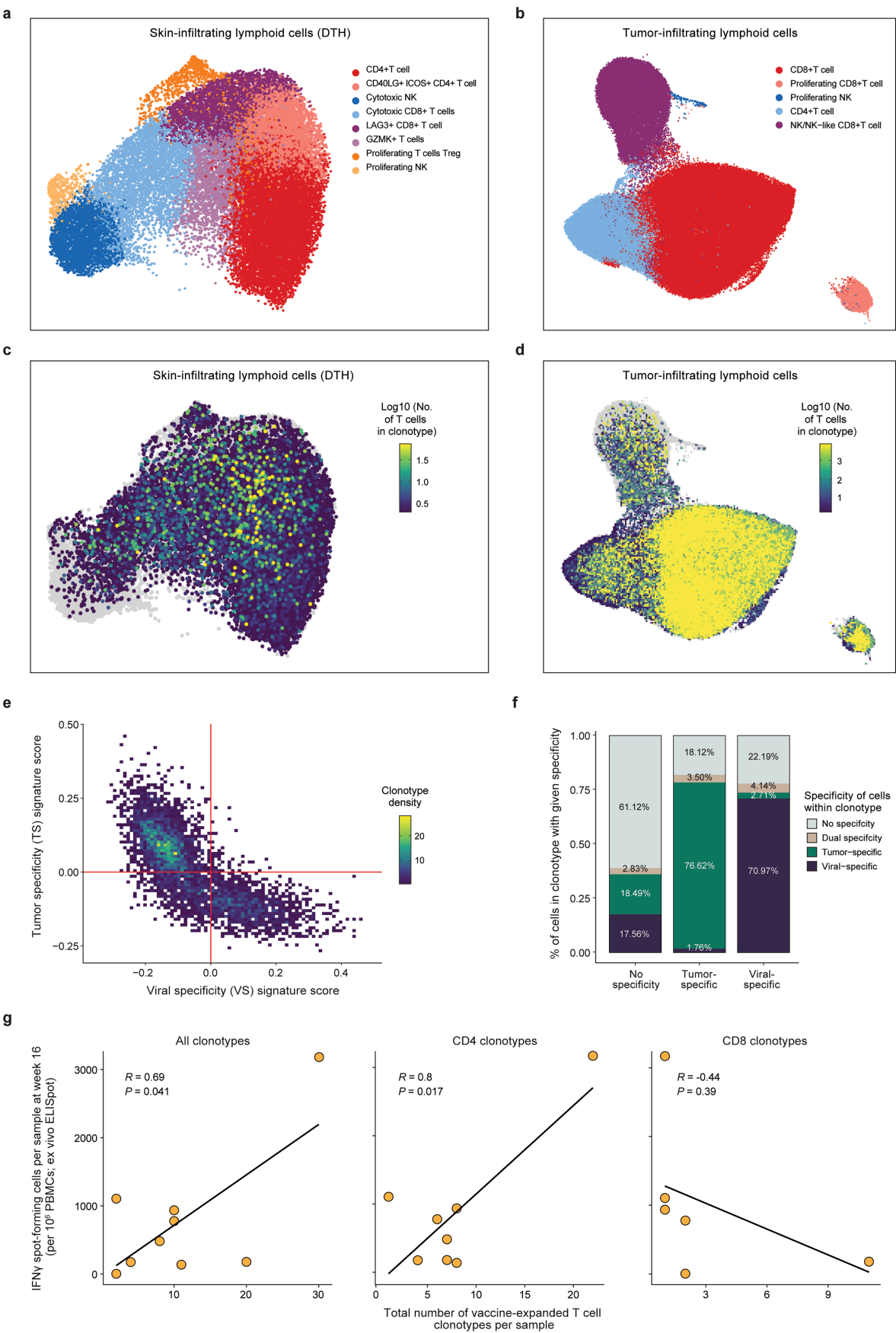
$n = 5$ patients who received vaccine + ipilimumab; boxplot hinges represent 25th to 75th percentiles, central lines represent the medians, the whiskers extend to lowest and highest values no greater than $1.5 \times$ interquartile range away from the 25th and 75th percentiles, and the dots indicate outliers).



Extended Data Fig. 8 | See next page for caption.

Extended Data Fig. 8 | Rapid and durable expansion of T cell clonotypes following vaccination. a, For each of the $n = 9$ patients with peripheral blood TCR sequencing data available, the dynamics of T cell clonotypes with inferred vaccine specificity is shown following vaccination. Vaccine-expanded clonotypes were defined as undetectable or at the lower limit of detection at baseline (week 0), expands by at least 10-fold after vaccination in all subsequent timepoints (including at least 3 unique molecular identifier sequencing reads at ≥ 2 timepoints), and is identified in the skin during the DTH assessment. (*left*), Each gray line represents one T cell clonotype, and the red line represents the

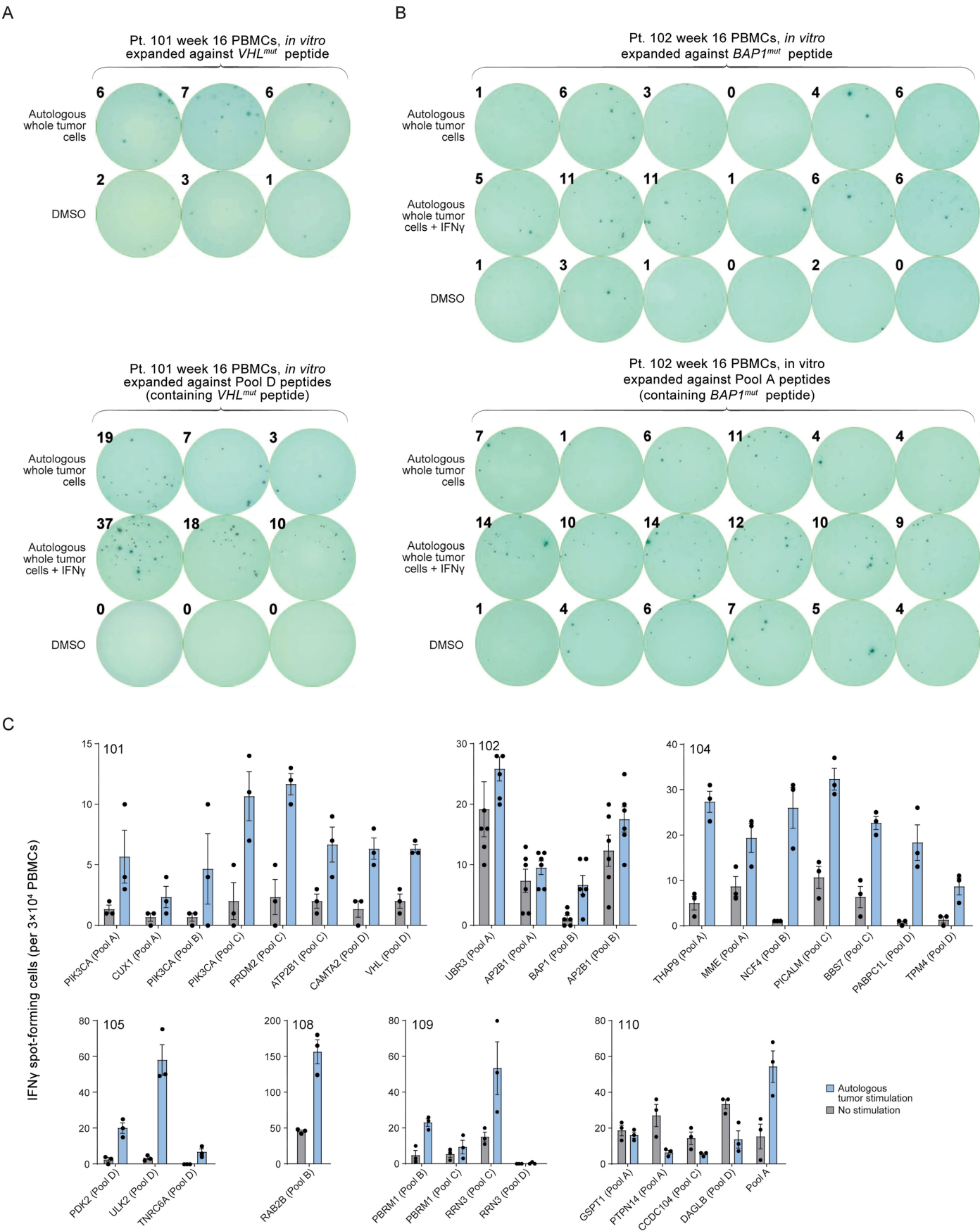
sum of all clonotypes for an individual patient. (*middle*) Each light blue line represents a CD4 clonotype, dark blue lines represent CD8 clonotypes, and gray represents unresolved clonotypes. (*right*) The summation of all clonotypes (red), all CD4 clonotypes (light blue), or all CD8 clonotypes (dark blue) for each patient. b, The mean (and standard error of the mean) vaccine-expanded TCR clonotype frequency over time for all $n = 9$ patients (linear scale). c, The median (and interquartile range) of vaccine-expanded TCR clonotype frequencies over time for all $n = 9$ patients (red), also shown for all CD4 clonotypes (light blue) and CD8 clonotypes (dark blue).



Extended Data Fig. 9 | See next page for caption.

Extended Data Fig. 9 | Inference of tumor-specific, viral-specific, and vaccine-specific T cell clonotypes. UMAP representations of scRNA-seq data from lymphoid cells in (a) the skin during the cutaneous delayed-type hypersensitivity (DTH) assessment, and (b) the tumor at the time of surgical resection. Single-cell TCR-sequencing of T cells showing areas of clonotype expansion in (c) the skin (during DTH assessment) and (d) the baseline tumor. e, For tumor-infiltrating T cells, the per-clonotype average expression of previously defined²⁸ gene signatures for tumor specificity (TS) and viral specificity (VS). The red lines indicate thresholds that were used to identify TS and VS T cells. f, For each clonotype that was assigned as TS or VS (or no

specificity), the percentage of individual T cells within that clonotype that express predominantly the TS signature, the VS signature, or neither (dual specificity of no specificity). Overall, for clonotypes that were labeled as TS or VS, over 70% of the individual T cells were concordant with that classification. g, association of expanded CD4 T cell clonotypes with IFN γ response after vaccination. The total number of inferred vaccine-expanded clonotypes (*left*), CD4-only clonotypes (*middle*), and CD8-only clonotypes (*right*) in each sample is plotted against the total number of IFN γ spot-forming cells by ex vivo ELISpot assessment at week 16 following vaccination (two-sided Pearson correlation).



Extended Data Fig. 10 | See next page for caption.

Extended Data Fig. 10 | Vaccine-reactive T cells can recognize autologous tumor cells. IFN γ + ELISpots from week 16 PBMCs stimulated with individual vaccine peptides (*top*) or pools of peptides (*bottom*), rested, and then re-stimulated with autologous tumor cells (which had been pre-treated with or without IFN γ + to improve antigen presentation). Representative ELISpots from peptides harboring driver mutations in (a) *VHL* and (b) *BAP1*. c, Autologous tumor-reactivity for each patient and each assayed peptide (and which pool it

was contained in). Each graph represents the absolute IFN γ ELISpot count (mean of triplicates with standard error of the mean). For Fig. 4f in the main text, a vaccine peptide considered to induce tumor-reactivity if it was significantly increased over the DMSO negative control (t-test) and had median spot count at least three-fold higher than the negative control. For patient 110, only T cells expanded using pool of vaccine peptides (pool A) were capable of recognizing autologous tumor cells.

Reporting Summary

Nature Portfolio wishes to improve the reproducibility of the work that we publish. This form provides structure for consistency and transparency in reporting. For further information on Nature Portfolio policies, see our [Editorial Policies](#) and the [Editorial Policy Checklist](#).

Statistics

For all statistical analyses, confirm that the following items are present in the figure legend, table legend, main text, or Methods section.

- | | |
|-------------------------------------|--|
| n/a | Confirmed |
| <input type="checkbox"/> | <input checked="" type="checkbox"/> The exact sample size (<i>n</i>) for each experimental group/condition, given as a discrete number and unit of measurement |
| <input type="checkbox"/> | <input checked="" type="checkbox"/> A statement on whether measurements were taken from distinct samples or whether the same sample was measured repeatedly |
| <input type="checkbox"/> | <input checked="" type="checkbox"/> The statistical test(s) used AND whether they are one- or two-sided
<i>Only common tests should be described solely by name; describe more complex techniques in the Methods section.</i> |
| <input type="checkbox"/> | <input checked="" type="checkbox"/> A description of all covariates tested |
| <input type="checkbox"/> | <input checked="" type="checkbox"/> A description of any assumptions or corrections, such as tests of normality and adjustment for multiple comparisons |
| <input type="checkbox"/> | <input checked="" type="checkbox"/> A full description of the statistical parameters including central tendency (e.g. means) or other basic estimates (e.g. regression coefficient) AND variation (e.g. standard deviation) or associated estimates of uncertainty (e.g. confidence intervals) |
| <input type="checkbox"/> | <input checked="" type="checkbox"/> For null hypothesis testing, the test statistic (e.g. <i>F</i> , <i>t</i> , <i>r</i>) with confidence intervals, effect sizes, degrees of freedom and <i>P</i> value noted
<i>Give P values as exact values whenever suitable.</i> |
| <input checked="" type="checkbox"/> | <input type="checkbox"/> For Bayesian analysis, information on the choice of priors and Markov chain Monte Carlo settings |
| <input checked="" type="checkbox"/> | <input type="checkbox"/> For hierarchical and complex designs, identification of the appropriate level for tests and full reporting of outcomes |
| <input type="checkbox"/> | <input checked="" type="checkbox"/> Estimates of effect sizes (e.g. Cohen's <i>d</i> , Pearson's <i>r</i>), indicating how they were calculated |

Our web collection on [statistics for biologists](#) contains articles on many of the points above.

Software and code

Policy information about [availability of computer code](#)

Data collection	No code was used for data collection.
Data analysis	<p>Somatic mutations in WES data were detected by an implementation of the Cancer Genome Analysis WES Characterization Pipeline (as implemented in Braun et al, Nature Med, 2020; hereafter, referred to as the CGA pipeline) in a cloud-based analysis platform, Terra (https://terra.bio/). We utilized version 0.2 of the CGA pipeline. As QC steps, the CGA pipeline ran deTiN (v1.8.5) and ContEst for estimating tumor-in-normal and cross-patient contaminations, respectively. The pipeline applies multiple artifact filters such as the read-realignment filter by BLAT and the read orientation bias filters followed by SNV and indel calling with MuTect and Strelka. All somatic alterations were annotated using Oncotator. Tumor ploidy and purity was determined using ABSOLUTE, and this was used to assign clonality (cancer cell fraction; CCF) for each somatic mutation. RNA-seq data were aligned to the human reference genome (hg19) and transcriptome (GENCODE v19) using STAR (v2.6.1), and expression was quantified (transcripts per million; TPM) using RSEM (v1.3.1). All coding mutations were visualized using the Integrated Genomics Viewer (IGV v2). Antigen prediction was performed using HLathena and NetMHCpan version 4 (eluted ligand rank). Flow cytometry data were acquired on a BD LSR Fortessa with FACSDiva and analyzed with Flow Jo (version 10.8.1). For scRNA-seq, the 10x Cell Ranger pipeline (version 6.1.2) was utilized for data demultiplexing, data alignment and count quantification, and TCR clonotype assembly. Single-cell RNA sequencing data were imported and read using a custom function built upon the Seurat 4.3.0 pipeline. doubletFinder (version 2.0.3), scDblFinder (version 1.12.0) were used for doublet detection. Harmony 0.1.1 was used for batch correction. We use clustree 0.5.0 for optimal clustering resolution. Heatmaps were generated using pheatmap v1.0.12. For TCR diversity and clonotype analysis, we utilized the R package VDJdive version 1.3.5 and scRepertoire (v1.8.0). For bulk TCR processing from PBMCs, code is available on GitHub at: https://github.com/Wu-Lab-DFCI-Harvard/bulkTCR_Script.</p> <p>Disease-free survival is reported as the time (in months) of disease recurrence or death from the start of treatment. Analysis and</p>

visualizations were generated using the R packages “survival” (v.3.5.5) and “survminer” (v0.4.9). The Kaplan-Meier curves for KEYNOTE-564 and IMmotion-010 were reconstructed using Digitizelt software (v2.5.9) together with the “IPDfromKM” package in R (v0.1.10).

For manuscripts utilizing custom algorithms or software that are central to the research but not yet described in published literature, software must be made available to editors and reviewers. We strongly encourage code deposition in a community repository (e.g. GitHub). See the Nature Portfolio [guidelines for submitting code & software](#) for further information.

Data

Policy information about [availability of data](#)

All manuscripts must include a [data availability statement](#). This statement should provide the following information, where applicable:

- Accession codes, unique identifiers, or web links for publicly available datasets
- A description of any restrictions on data availability
- For clinical datasets or third party data, please ensure that the statement adheres to our [policy](#)

The list of somatic mutations for all patients (mutation annotation file) is available in Table S1. The IFN γ ELISpot responses for ex vivo peptide pool stimulation, in vitro individual peptide stimulation, and autologous tumor testing are available in Table S2. The median normalized protein expression (NPX) values of circulating soluble proteins is available in Table S3. The cell numbers and T cell clonotype metrics from scRNA-seq and TCR-seq of skin samples is available in Table S4. The T cell clonotype metrics for tumor-infiltrating T cells and for peripheral T cells are available in Table S5. The individual T cell clonotypes and their corresponding phenotypes are available in Table S6. The reference genome (hg19) and transcriptome (GENCODE v19) are publicly available ([gs://firecloud-tcga-open-access/tutorial/reference/annotation.db.ucsc.hg19.tar](https://firecloud-tcga-open-access/tutorial/reference/annotation.db.ucsc.hg19.tar) and [gs://firecloud-tcga-open-access/tutorial/reference/rna-seq/gencode.v19.genes.v7_model.patched_contigs.gtf](https://firecloud-tcga-open-access/tutorial/reference/rna-seq/gencode.v19.genes.v7_model.patched_contigs.gtf), respectively). All raw DNA and RNA sequencing files for the tumor samples are deposited in dbGaP (phs003710.v1.p1).

Research involving human participants, their data, or biological material

Policy information about studies with [human participants or human data](#). See also policy information about [sex, gender \(identity/presentation\), and sexual orientation](#) and [race, ethnicity and racism](#).

Reporting on sex and gender	Self-reported sex was described for all study participants. Of the 9 patients in the current study, 7 were self-reported as males and 2 as females. This roughly reflects the increased prevalence of renal cell carcinoma among men.
Reporting on race, ethnicity, or other socially relevant groupings	Self-reported race and ethnicity were collected as part of the medical record.
Population characteristics	Age, demographic information, and tumor characteristics were collected from the medical records. Age, performance status, tumor histology, stage, grade, and size were reported. Age: median 65.5 years, range 50.4 - 75.7 years. Sex: 22% female, 78% male. ECOG performance status: 78% 0, 22% 1 Tumor histology: 100% clear cell Stage: 78% stage III, 22% stage IV ISUP grade: 11% grade 2, 89% grade 3 Primary tumor size: 44% 4-7cm, 33% 7-10cm, 22% > 10cm Prior treatment: none
Recruitment	All potentially eligible subjects (renal mass, clinical T3 or T4 with plan for resection, no obvious exclusions) seen at the Dana-Farber Cancer Institute medical oncology clinic by participating oncologists, or at the Brigham and Women's Hospital urology clinic by participating urologists, were identified and provided an opportunity to consent and screen for the trial. Study eligibility included age \geq 18, ECOG performance status \leq 1, suspected stage III or IV clear cell renal cell carcinoma (at initial registration; confirmed stage III or IV clear cell renal cell carcinoma at secondary registration), undergoing curative intent surgery (nephrectomy and/or metastasectomy to no evidence of disease), no active autoimmune disease, and no prior therapy with immunomodulatory agents. A potential source of bias is that patients who were not seen by participating medical oncologists and urologists would not participate in the trial.
Ethics oversight	Dana-Farber / Harvard Cancer Center (DF/HCC) Institutional Review Board.

Note that full information on the approval of the study protocol must also be provided in the manuscript.

Field-specific reporting

Please select the one below that is the best fit for your research. If you are not sure, read the appropriate sections before making your selection.

- ☒ Life sciences ☐ Behavioural & social sciences ☐ Ecological, evolutionary & environmental sciences

For a reference copy of the document with all sections, see nature.com/documents/nr-reporting-summary-flat.pdf

Life sciences study design

All studies must disclose on these points even when the disclosure is negative.

Sample size	This was a phase I study of safety and tolerability of this vaccination strategy in renal cell carcinoma. The initial cohort size of patients treated with vaccine + ipilimumab was designed to identify dose-limiting toxicity (DLT). If the true but unknown rate of dose-limiting toxicity is low, i.e., 10%, the probability of observing either no DLTs or a single DLT in 5 patients is 0.92. The sample. With the study design, observing more than a single DLT was unacceptable. Additionally, sample size was designed to identify toxicities of out interest. For 5 patients treated with vaccine plus ipilimumab, if the true but known probability of toxicity is 0.1, 0.2, 0.3, 0.4, or 0.5, the probability of observing it in at least 1 of 5 patients would be 0.41, 0.67, 0.83, 0.92, or 0.97, respectively. For the secondary endpoint of induction of IFN γ T cell response, we estimated that there would be approximately 100 peptides among patients treated with vaccine plus ipilimumab, and at least 40 patients treated with vaccine alone. Then, using a Fischer exact test, and assuming a low rate of 5% CD8+ response in the vaccine alone group, we would have 90% power to detect a 25% increase in CD8+ T cell response. All sample size calculations for the original clinical trial are provided in the protocol, as part of Supplementary Information.
Data exclusions	The current studies reports on the first 9 patients treated on study with sufficient follow-up (n = 5 treated with vaccination plus ipilimumab, and n = 4 with vaccination alone). As noted in the methods, a third cohort (vaccination plus a higher dose of ipilimumab) was accrued until December 2022 with follow-up ongoing, and results of that immature cohort are not reported here.
Replication	This study used exclusively primary human material from participants in the trial, and so replication was not typically performed. For flow cytometry, Olink analysis, and all sequencing studies (single-cell RNA-sequencing, TCR sequencing), no replication was performed. For the IFN γ ELISpot, we performed technical replicates (triplicate). Results from each replicate is provided in supplementary table S2.
Randomization	There was no randomization in this phase I clinical study. Specifically, randomization is not applicable to this individual cohort, phase I clinical trial. Of note, there is formal comparison between arms in the main figures of this study (and therefore, no adjustment for covariates).
Blinding	There was no blinding in this phase I clinical study, as there was no randomization. Investigators performing the flow cytometry, IFN γ ELISpots, and single-cell analysis directly were blinded to clinical outcomes.

Reporting for specific materials, systems and methods

We require information from authors about some types of materials, experimental systems and methods used in many studies. Here, indicate whether each material, system or method listed is relevant to your study. If you are not sure if a list item applies to your research, read the appropriate section before selecting a response.

Materials & experimental systems

Methods

n/a	Involved in the study	n/a	Involved in the study
<input type="checkbox"/>	<input checked="" type="checkbox"/> Antibodies	<input checked="" type="checkbox"/>	<input type="checkbox"/> ChIP-seq
<input checked="" type="checkbox"/>	<input type="checkbox"/> Eukaryotic cell lines	<input type="checkbox"/>	<input checked="" type="checkbox"/> Flow cytometry
<input checked="" type="checkbox"/>	<input type="checkbox"/> Palaeontology and archaeology	<input checked="" type="checkbox"/>	<input type="checkbox"/> MRI-based neuroimaging
<input checked="" type="checkbox"/>	<input type="checkbox"/> Animals and other organisms		
<input type="checkbox"/>	<input checked="" type="checkbox"/> Clinical data		
<input checked="" type="checkbox"/>	<input type="checkbox"/> Dual use research of concern		
<input checked="" type="checkbox"/>	<input type="checkbox"/> Plants		

Antibodies

Antibodies used	<p>All flow cytometry antibodies were purchased from BD Biosciences or BioLegend:</p> <p>CD3 (clone UCHT1, APC-Cy7, Biolegend cat#300426) - dilution 1:20 per million PBMC/100uL.</p> <p>CD4 (clone L200, PerCP-Cy5.5, BD Biosciences cat#552838) - dilution 1:5 per million PBMC/100uL.</p> <p>CD8 (clone RPA-T8, AlexaFluor-488, BD Biosciences cat#557696) - dilution 1:20 per million PBMC/100uL.</p> <p>CD45RO (clone UCHL1, PE, BD Biosciences cat#555493) - dilution 1:5 per million PBMC/100uL.</p> <p>PD-1 (clone EH12.2H7, BrilliantViolet 785, Biolegend cat#329930) - dilution 1:40 per million PBMC/100uL.</p> <p>IFN-gamma (clone B27, APC-R700, BD Biosciences cat#564981) - dilution 1:20 per million PBMC/100uL.</p> <p>TNF (clone MAb11, PE-Cy7, BD Biosciences cat#560923) - dilution 1:20 per million PBMC/100uL.</p> <p>IL-2 (clone MQ1-17H12, BrilliantViolet 605, BD Biosciences cat#564165) - dilution 1:20 per million PBMC/100uL.</p> <p>For ELISpot, antibodies were purchased from Mabtech:</p> <p>For capture (primary antibody), plates were coated with IFN-gamma antibody (Mabtech, clone 1-D1K, cat#3420-3-250) - dilution 1:500.</p> <p>For detection (secondary antibody), anti-human IFN-gamma antibody was used (Mabtech, clone 7-BG-1 biotin, cat#3420-6-250) - dilution 1:1000</p>
Validation	All antibodies used in the manuscript were purchased from reputable commercial vendors, and all validation studies were performed by the commercial vendors themselves. Additional information on validation can be found on the manufacturers' websites, listed below.

All flow cytometry antibodies were purchased from BD Biosciences or BioLegend:

CD3 (clone UCHT1, APC-Cy7, Biolegend cat#300426) - <https://www.biolegend.com/en-gb/clone-search/apc-cyanine7-anti-human-cd3-antibody-3929?GroupID=BLG5900>

CD4 (clone L200, PerCP-Cy5.5, BD Biosciences cat#552838) - <https://www.bdbiosciences.com/en-us/products/reagents/flow-cytometry-reagents/research-reagents/single-color-antibodies-ruo/percp-cy-5-5-mouse-anti-human-cd4.552838>

CD8 (clone RPA-T8, AlexaFluor-488, BD Biosciences cat#557696) - <https://www.bdbiosciences.com/en-us/products/reagents/flow-cytometry-reagents/research-reagents/single-color-antibodies-ruo/alexa-fluor-488-mouse-anti-human-cd8.557696>

CD45RO (clone UCHL1, PE, BD Biosciences cat#555493) - <https://www.bdbiosciences.com/en-us/products/reagents/flow-cytometry-reagents/research-reagents/single-color-antibodies-ruo/pe-mouse-anti-human-cd45ro.555493>

PD-1 (clone EH12.2H7, BrilliantViolet 785, Biolegend cat#329930) - <https://www.biolegend.com/nl-nl/products/brilliant-violet-785-anti-human-cd279-pd-1-antibody-7980>

IFN-gamma (clone B27, APC-R700, BD Biosciences cat#564981) - <https://www.bdbiosciences.com/en-us/products/reagents/flow-cytometry-reagents/research-reagents/single-color-antibodies-ruo/apc-r700-mouse-anti-human-ifn.564981>

TNF (clone MAb11, PE-Cy7, BD Biosciences cat#560923) - <https://www.bdbiosciences.com/en-eu/products/reagents/flow-cytometry-reagents/research-reagents/single-color-antibodies-ruo/pe-cy-7-mouse-anti-human-tnf.560923>

IL-2 (clone MQ1-17H12, BrilliantViolet 605, BD Biosciences cat#564165) - <https://www.bdbiosciences.com/en-us/products/reagents/flow-cytometry-reagents/research-reagents/single-color-antibodies-ruo/bv605-rat-anti-human-il-2.564165>

For ELISpot, antibodies were purchased from Mabtech:

For capture (primary antibody), plates were coated with IFN-gamma antibody (Mabtech, clone 1-D1K, cat#3420-3-250) - <https://www.mabtech.com/products/anti-human-ifn-g-mab-1-d1k-unconjugated-3420-3>

For detection (secondary antibody), anti-human IFN-gamma antibody was used (Mabtech, clone 7-BG-1 biotin, cat#3420-6-250) - <https://www.mabtech.com/products/3420-6>

Clinical data

Policy information about [clinical studies](#)

All manuscripts should comply with the ICMJE [guidelines for publication of clinical research](#) and a completed [CONSORT checklist](#) must be included with all submissions.

Clinical trial registration	NCT02950766
Study protocol	The study protocol is included in the supplementary appendix.
Data collection	Data was collected as described in the Methods section. Patients were enrolled in the first cohort (vaccine plus 2.5mg of subcutaneous ipilimumab at each vaccine site) and the second cohort (vaccine alone) between March 2019 and September 2021. Clinical outcome and safety data are reported until the clinical data cutoff of July 7, 2023. Data was collected at Dana-Farber Cancer Institute and Brigham and Women's Hospital during and beyond the enrollment period.
Outcomes	<p>Primary Objectives:</p> <p>To evaluate safety and tolerability of administering NeoVax and locally delivered Ipilimumab in patients with fully resected, high-risk clear cell renal cell carcinoma (ccRCC).</p> <p>To determine the maximum tolerated dose (MTD) of locally administered Ipilimumab when delivered with NeoVax.</p> <p>Secondary Objectives</p> <p>To assess the induction of neoantigen-specific cellular immune responses following administration of NeoVax with Ipilimumab.</p> <p>To determine the proportion of patients alive without recurrence at two years after surgery following administration of NeoVax with Ipilimumab.</p>

Plants

Seed stocks	N/A
Novel plant genotypes	N/A
Authentication	N/A

Flow Cytometry

Plots

Confirm that:

- ☒ The axis labels state the marker and fluorochrome used (e.g. CD4-FITC).
- ☒ The axis scales are clearly visible. Include numbers along axes only for bottom left plot of group (a 'group' is an analysis of identical markers).
- ☒ All plots are contour plots with outliers or pseudocolor plots.
- ☒ A numerical value for number of cells or percentage (with statistics) is provided.

Methodology

Sample preparation

PBMCs were thawed and rested overnight at 37°C in RPMI (Life Technologies) containing 10% human serum (Sigma-Aldrich), 1% penicillin and streptomycin (Life Technologies), and 20ng/mL of IL-7 (Peprotech). The following day PBMCs were stimulated with vaccine peptide pools (2µg/mL per individual peptide) in completed R10 media (RPMI, 10% FBS, 1% Pen/Strep). After one hour of co-culture at 37°C, transport inhibitors GolgiStop and GolgiPlug were added. Following 5 hours of incubation at 37°C, samples were washed with 1X PBS and stained with live/dead dye in 1X PBS for 20 min at 4°C. Samples were subsequently washed with Staining buffer (1X PBS, 10% FBS, 1% penicillin and streptomycin). Fc receptors were blocked for 15 min at 4°C with Human TruStain FcX in staining buffer. Surface staining antibodies were then added: CD4 (clone L200), CD8 (clone RPA-T8), CD45RO (clone UCHL1), and PD-1 (clone EH12.2H7). Following 30 minutes of incubation at 4°C, samples were washed twice before fixation and permeabilized with CytoFix/CytoPerm for 15 minutes at 4°C. Samples were then washed twice and resuspended in 1X Perm/Wash buffer to conduct intracellular staining with: IFN-γ (clone B27), TNF (clone Mab11), IL-2 (clone MQ1-17H12), and CD3 (clone UCHT1). Following 30 minutes of incubation at 4°C, samples were washed twice with Perm/Wash, once with staining buffer, and then resuspended in CytoFix fixation buffer until acquisition. All flow reagents were purchased from BD Biosciences or Biolegend.

Instrument

Data were acquired on a BD LSR Fortessa.

Software

Data was acquired on the BD LSR Fortess with FACSDiva, and then all analysis was performed with Flow Jo (version 10.8.1)

Cell population abundance

There was no post-sort population analyzed in this study. Gating was performed as described in Extended Data Figure 4.

Gating strategy

Gating was performed as described in Extended Data Figure 4. Brief, after gating on live cells (BioLegend Zombie Yellow negative), a lymphocyte gate was drawn using FSC/SSC. Doublets/multitplets were excluded by gating in FSC-A vs FSC-H and SSC-A vs SSC-H. CD3+ T cells were gated, and then CD4 vs CD8 cells wete gated and analyzed separately. For CD4 T cells, gates were drawn on CD4 vs each individual cytokine (IFNgamma, TNF, or IL-2). This process was repeated for CD8 T cells. For PD-1 and CD45RO, median fluorescence intensity (MFI) was reported.

- ☒ Tick this box to confirm that a figure exemplifying the gating strategy is provided in the Supplementary Information.